IMMOBILIZATION OF BATHOPHENANTHROLINE ON MODIFIED MESOPOROUS SILICA FILM FOR DETERMINATION OF NICKEL ION

NICHAKORN PORNNONGSAN

A Thesis Submitted in Partial Fulfillment of the Requirements for the

Degree of Master of Science in Chemistry

Suranaree University of Technology

Academic Year 2022

การตรึงบาโทฟีแนนโทรลีนซัลโฟเนตบนฟิล์มซิลิกาเมโซพอร์ที่ดัดแปร
สำหรับการหาปริมาณไอออนนิกเกิล

นางสาวณิชากร พรหนองแสน

วิทยานิพนธ์นี้เป็นส่วนหนึ่งของการศึกษาตามหลักสูตรปริญญาวิทยาศาสตรมหาบัณฑิต
สาขาวิชาเคมี
มหาวิทยาลัยเทคโนโลยีสุรนารี
ปีการศึกษา 2565

IMMOBILIZATION OF BATHOPHENANTHROLINE ON MODIFIED
MESOPOROUS SILICA FILM FOR DETERMINATION OF NICKEL ION

Suranaree University of Technology has approved this thesis submitted in partial fulfillment for a Master's Degree.

Thesis Examining Committee

_____

(Assoc. Prof. Dr. Anyanee Kamkaew)

Chairperson

_____

(Assoc. Prof. Dr. Sanchai Prayoonpokarach)

Member (Thesis Advisor)

_____

(Prof. Dr. Jatuporn Wittayakun)

Member

_____
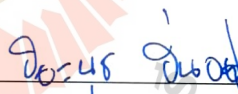
(Dr. Piyanut Pinyou)

Member

_____

(Asst. Prof. Dr. Sirinuch Loiha)

Member

_____   _____

(Assoc. Prof. Dr. Chatchai Jothityangkoon)   (Prof. Dr. Santi Maensiri)

Vice Rector for Academic Affairs   Dean of Institute of Science

and Quality Assurance

ณิชากร พรหนองแสน : การตรึงบาโทฟีแนนโทรลีนซัลโฟเนตบนฟิล์มซิลิกาเมโซพอร์ที่ดัด
แปรสำหรับการหาปริมาณไอออนนิกเกิล (IMMOBILIZATION OF
BATHOPHENANTHROLINE ON MODIFIED MESOPOROUS SILICA FILM FOR
DETERMINATION OF NICKEL ION) อาจารย์ที่ปรึกษา : รองศาสตราจารย์ ดร. สัญชัย
ประยูรโภคราช, 73 หน้า

คำสำคัญ: ฟิล์มซิลิกาเมโซพอร์, บาโทฟีแนนโทรลีนไดซัลโฟเนต, ไอออนนิกเกิล, ฟลูออเรสเซนซ์

วิทยานิพนธ์นี้ ประสบความสำเร็จในการพัฒนาเซ็นเซอร์เคมีเชิงแสงสำหรับการหาปริมาณ
ไอออนนิกเกิลภายใต้การตรึงบาโทฟีแนนโทรลีนไดซัลโฟเนตบนฟิล์มซิลิกาเมโซพอร์ที่ดัดแปร วิธีการ
ประกอบตัวเองร่วมกับการช่วยทางเคมีไฟฟ้านำมาใช้ในการเตรียมฟิล์มซิลิกาเมโซพอร์บนแผ่นแก้วที่
เคลือบด้วยทินออกไซด์เจือด้วยฟลูออรีน โดยที่ช่องเมโซพอร์ที่จัดเรียงอย่างเป็นระเบียบสูงและมี
ความหนาแตกต่างกัน ฟิล์มที่สังเคราะห์ได้นำมาวิเคราะห์ลักษณะด้วยเทคนิคไซคลิกโวลแทมเมตรี
เทคนิคจุลทรรศน์อิเล็กตรอนแบบส่องกราด เทคนิคจุลทรรศน์อิเล็กตรอนแบบส่องผ่าน และเทคนิคฟู
เรียร์ทรานส์ฟอร์มอินฟราเรดสเปกโทรสโกปี
ฟิล์มชั้นเดียวและหลายชั้นนำมาดัดแปรด้วย 3-อะมิโนโพรพิล ไตรเอทอกซีไซเลนเพื่อใช้เป็น
วัสดุรองรับการตรึงบาโทฟีแนนโทรลีนไดซัลโฟเนต ซึ่งวิธีดัดแปรที่ใช้คือวิธีการควบแน่นร่วมกันใน
กระบวนการสังเคราะห์ และวิธีโพส์ตกราฟติง ฟิล์มที่ดัดแปรหมู่อะมิโนด้วยวิธีโพส์ตกราฟติงสามารถ
ตรึงบาโทฟีแนนโทรลีนไดซัลโฟเนตได้มากกว่า ฟิล์มที่ตรึงบาโทฟีแนนโทรลีนไดซัลโฟเนตนำมาเคลือบ
ด้วยแนฟฟิออนเพื่อป้องกันการหลุดออกของบาโทฟีแนนโทรลีนไดซัลโฟเนต ฟิล์มเซ็นเซอร์เคลือบ
ด้วยแนฟฟิออนเกิดการคายแสงที่ความยาวคลื่น 395 นาโนเมตร เมื่อกระตุ้นที่ความยาวคลื่น 285 นา
โนเมตร ฟิล์มเซ็นเซอร์ที่พัฒนาขึ้นมามีลักษณะเป็นเนื้อเดียวกัน โปร่งใส มีความเสถียรทางกายภาพ
ฟิล์มเซ็นเซอร์เคลือบด้วยแนฟฟิออนเมื่ออยู่ในสารละลายนิกเกิลที่พีเอช 6 จะเกิดการยับยั้งแสงฟลูออ
เรสเซนซ์ วิธีที่พัฒนาขึ้นมาตรวจวัดไอออนนิกเกิลให้กราฟมาตรฐานที่เป็นเส้นตรงในช่วงความเข้มข้น
5 ถึง 40 ppm และมีขีดจำกัดการตรวจวัดที่ 2.45 ppm เซ็นเซอร์ที่พัฒนาขึ้นมาสามารถคืนสภาพได้
ในสารละลายอีดีทีเอ

สาขาวิชาเคมี	ลายมือชื่อนักศึกษา___ณิชากร พรหนองแสน___
ปีการศึกษา 2565	ลายมือชื่ออาจารย์ที่ปรึกษา_____

NICHAKORN PORNNONGSAN : IMMOBILIZATION OF BATHOPHENANTHROLINE ON MODIFIED MESOPOROUS SILICA FILM FOR DETERMINATION OF NICKEL ION. THESIS ADVISOR : ASSOC. PROF. SANCHAI PRAYOONPOKARACH, Ph.D. 73 PP.

In this thesis, the successful development of an optical chemical sensor for the determination of Ni^{2+} ions were achieved through the immobilization of bathophenanthroline disulfonate (BPS) on a modified mesoporous silica film. Electrochemically assisted self-assembly was employed to prepare highly oriented mesochannel MSFs of various thicknesses on fluorine-doped tin oxide coated glass. Cyclic voltammetry, scanning electron microscopy, transmission electron microscopy, and Fourier transform infrared spectroscopy were used to characterize the films.

The single- and multiple-layered films were modified with 3-aminopropyl triethoxysilane by co-condensation in the synthesis mixture and post-grafting to be used as supporting material for immobilizing BPS. More BPS was immobilized on the amino-modified films from the post-grafting method. Nafion was used to coat BPS-immobilized films to prevent BPS leaching. The Nafion-coated sensing films showed an emission wavelength of 395 nm with an excitation wavelength of 285 nm. The developed sensing films were homogeneous, transparent, and physically stable. The Nafion-coated sensing film exhibited fluorescence quenching upon exposure to Ni^{2+} solutions at pH 6. The developed method provided a linear calibration for Ni^{2+} concentration in the 5-40 ppm range and the detection limit of 2.45 ppm. The developed sensing film could be regenerated in an EDTA solution.

School of Chemistry

Academic Year 2022

Student's Signature ณิชากร พรหนองแส่น

Advisor's Signature

ACKNOWLEDGEMENTS

CONTENTS

CONTENTS (Continued)

CONTENTS (Continued)

LIST OF TABLES

LIST OF FIGURES

LIST OF FIGURES (Continued)

LIST OF FIGURES (Continued)

CHAPTER I

INTRODUCTION

1.1 Monitoring nickel contamination

Nickel is a heavy metal that can be found contaminating the environment, soil, and water at low concentrations. However, it can pose a risk to human health when individuals are exposed to nickel at a concentration higher than the maximum tolerable amount. The metal plating, mining, and battery industries are some of the contributors to the environmental contamination of nickel. Nickel compounds can accumulate in the human body through various means, such as breathing air, drinking water, eating food, or working in nickel-related industries. Exposure to large quantities of nickel can cause severe health problems such as skin allergies, fibrosis, and respiratory tract cancer (Amini et al., 2004). The World Health Organization (WHO) and the United States Environmental Protection Agency (EPA) regulated the concentration of nickel in drinking water not to exceed 0.07 and 0.04 ppm, respectively (Aragay et al., 2011). Therefore, it is necessary to regularly monitor and determine nickel concentration to ensure compliance with these regulations.

Techniques for the determination of nickel are, for example, atomic absorption spectroscopy (AAS), inductively coupled plasma atomic emission spectroscopy (ICP-AES), inductively coupled plasma-mass spectrometry (ICP-MS), and X-ray fluorescence spectroscopy (XRF) (Korent Urek et al., 2013). All of these methods are highly sensitive, accurate, and precise. However, they require expensive analytical instruments, trained personnel, and high operating costs. Therefore, alternative methods with fast and simple analysis and inexpensive operating costs for determining nickel are highly desirable.

1.2 Optical chemical sensor development

Spectroscopic methods have been developed to detect heavy metal ions in solutions. They rely on sensing reagents, commonly organic dyes, that can change their optical properties, including absorption and fluorescence, upon interaction with the analyte (Korent Urek et al., 2013). However, recovering and reusing the sensing reagent from the analytical sample solutions are difficult. Therefore, immobilizing the sensing reagent onto material support offers a good alternative for developing optical chemical sensors. This approach enables the reuse of the expensive sensing reagent and reduces chemical waste in the laboratory. Thin membranes have been used to immobilize sensing reagents, such as acetyl cellulose (Ensafi et al., 2003), Nafion (Amini et al., 2004), poly(vinyl chloride) (Aksuner et al., 2012; Shamsipur et al., 2004), agarose (Hashemi et al., 2011; Rasolzadeh et al., 2019). In this work, mesoporous silica film (MSF) was chosen as the supporting material for immobilizing the sensing reagent due to its high surface area, porosity, silanol surface available for modification with organic functional groups, and excellent chemical and thermal stability (Feng et al., 2013). Moreover, MSF can be synthesized on glass substrates, providing transparent films suitable for spectroscopic measurements.

Several methods have been developed for the preparation of MSF onto various solid substrates, including evaporation-induced self-assembly (EISA) (Urbanova et al., 2014), Stöber-solution growth (Teng et al., 2012) and electrochemically assisted self-assembly (EASA) (Walcarius et al., 2007). Stöber solution growth and EASA approaches are mostly used to generate mesochannels perpendicular to the substrate surface, which is an ideal configuration for achieving great accessibility and fast transport rates. The Stöber solution growth approach involves film formation using silica precursors with surfactant templates in an aqueous ethanol solution, gradually transforming at 60-100 °C. However, the drawback of this method is the long deposition time, 1-3 days (Teng et al., 2012), leading to the development of the EASA method, which is much faster, 5-30 s for film deposition, and can be operated at room temperature (Walcarius

et al., 2007). However, a substrate with a conducting surface is required for the EASA method.

The principle of the EASA method is basically the application of a suitable cathodic potential to an electrode immersed in a sol mixture of a silica source, i.e., tetraethyl orthosilicate, TEOS, and a surfactant template, i.e., cetyltrimethylammonium bromide (CTAB) in an acid solution of water and ethanol. The application of the potential results in reduction reactions at the electrode surface, which involve a proton (H^+), water (H_2O), and nitrate (NO_3^-), generating a hydroxide ion (OH^-). The hydroxide ion acts as a catalyst in the polycondensation of the sol, leading to the formation of templated silica mesopores with perpendicular channels on the electrode surface. The films synthesized using this method have a thickness ranging from 25-150 nm (Goux et al., 2009).

As is well-known, the enhancement of the sensing performance can be achieved by increasing the reaction area or surface area. The thickness of MSFs can be adjusted by extending the deposition time, increasing the applied current, increasing the cathodic applied potential, and raising the precursor concentration. However, excessively high cathodic potential or deposition time can result in a cracking film upon drying due to the shrinkage effect, and unwanted silica aggregates can form over the thin film (Ding et al., 2015; Giordano et al., 2017). A suitable potential can be sequentially applied to generate multi-layered films up to a thickness of 400 nm without aggregates and cracks (Giordano et al., 2017). Thicker MSF films provide more surface area, which is important for surface modification to accommodate target species or sensing reagents in sensor applications.

The sensing reagent plays a central role in designing optical chemical sensors and is commonly used in the spectrophotometric determination of various metal ions. One such sensing reagent is 4,7-diphenyl-1,10-phenanthroline disulfonic acid disodium salt, also known as bathophenantroline disulfonate (BPS). BPS can form a complex with metal ions, causing fluorescence quenching in the solution. However, it can be challenging to recover and reuse the sensing reagent.

This work aims to develop an optical chemical sensor with the reusability of the sensing reagent via immobilizing BPS on modified MSF supported by FTO-coated glass. The MSFs with various thicknesses were synthesized on FTO using the EASA method. The films were modified with 3-aminopropyl triethoxysilane as a support material for immobilizing BPS and testing their ability to accommodate the dye. Several factors affecting BPS immobilization were investigated, including film thickness, amino modification method (co-condensation and post-grafting), pH, and BPS immobilization time. Finally, the BPS-immobilized MSFs were further investigated as a potential optical chemical sensor for detecting nickel ions.
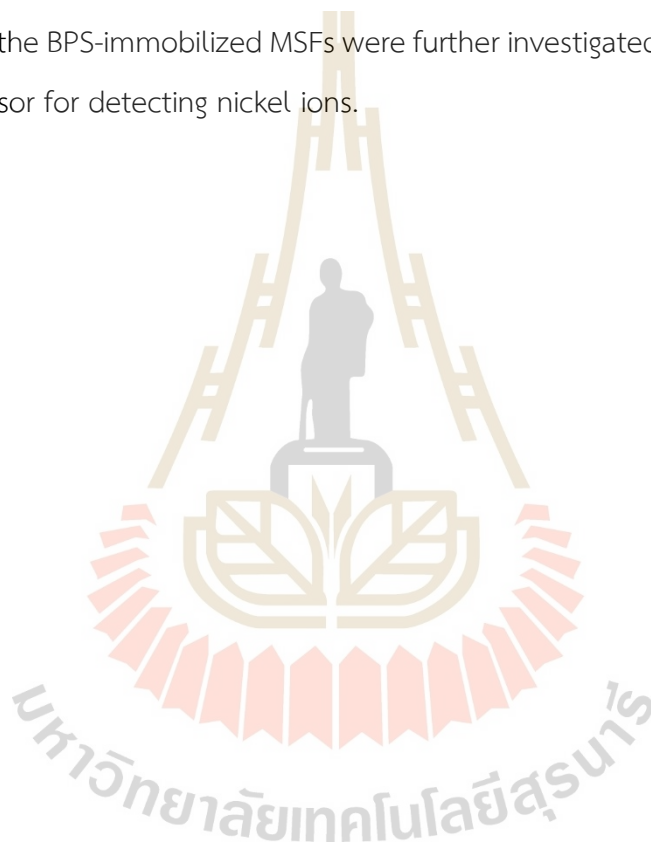
CHAPTER II

LITERATURE REVIEW

2.1 Optical chemical sensors for nickel ion

Nickel is a heavy metal widely used in many industrial and catalytic processes and can contaminate the environment, soil, and water. Nickel is known to be found in the environment at low concentrations, ppb-ppm levels. It can pose a risk to human health when individuals are exposed to high concentration levels. Therefore, it is important to regularly monitor and determine the concentration of nickel ions in water and environmental samples to ensure compliance with regulations. Several techniques are used for the determination of nickel, for example, atomic absorption spectroscopy, inductively coupled plasma atomic emission spectroscopy, inductively coupled plasma-mass spectrometry, and X-ray fluorescence spectroscopy (Aksuner et al., 2012). All of these methods provide high sensitivity, accuracy, and precision. However, they require expensive analytical instruments, trained personnel, and high operating cost. Due to the drawbacks associated with these methods, optical chemical sensors have been developed and can be alternatives for metal ion determination. The sensors can offer advantages such as highly selective, high sensitivity, rapid analysis results, simplicity, and cost-effectiveness.

Optical chemical sensors are a type of chemical sensor that can transform light rays containing chemical information into useful analytical signals through a transduction unit (Ahuja et al., 2012). These sensors typically rely on sensing reagents, such as organic dyes, immobilized on the surface of supporting materials. When the sensing reagent with the analyte, it can change optical properties, such as absorption an fluorescence, which can be correlated to the concentration of the analyte (Korent Urek et al., 2013). Suitable supporting materials, sensing reagents, and immobilization

techniques are critical for designing an optical chemical sensor to detect a given analyte. Consequently, this research focuses on developing an optical chemical sensor consisting of a sensing reagent immobilized on a selected support material to respond specifically to nickel ions (Ni^{2+}).

2.2 Sensing reagents for nickel ion

Sensing reagents are an essential part of developing optical chemical sensors. They play a vital role in detecting specific analytes in a sample by changing their optical properties upon interacting with the analytes. Various sensing reagents for optode membranes have been developed for many heavy metal ions. The reagent is typically immobilized onto or into the solid support through chemical bonding, electrostatic attraction, incorporation, or entrapment (Amini et al., 2004). Some published optical chemical sensors for Ni^{2+} determination were compared in terms of sensing reagent, matrix material, mode of measurement, detection limit, and response time, as shown in Table 2.1.

Sensing reagents used are either commercial (Amini et al., 2004; Hashemi et al., 2011; Shamsipur et al., 2004) or synthesized chemicals (Aksuner et al., 2012; Ensafi and Bakhshi, 2003; Rasolzadeh et al., 2019). Commercial reagents have the advantage over synthesized reagents regarding their availability, although selectivity to the analyte could be the weakness. The synthesized reagents are designed for specific analytes; therefore, the selectivity is superior to the commercial reagents. However, the synthesis of the sensing reagents involves complicated procedures. The product yield is typically low, which can be an issue for upscaling.

Table 2.1 Some optical chemical sensors for nickel ions.

Sensing reagent	Supporting matrix	Mode of measurement	Limit of detection	Response time
2-amino-1-cyclopentene-1-dithiocarboxylic acid[a]	Acetyl cellulose membrane	Absorbance	5.2×10^{-7} M	10 min
2,5-thiophenylbis(5-tert-butyl-1,3-benzexazole)[b]	PVC membrane	Fluorescence	8.0×10^{-9} M	< 40 s
2-(5-bromo-2-pyridylazo)-5-(diethylamino)phenol[c]	Nafion membrane	Absorbance	2.0×10^{-7} M	3 min
3,7-diamine-5-phenothiazoniom thionineacetate[d]	Agarose membrane	Absorbance	9.3×10^{-11} M	3 min
2-6-(3-methyl-3-mesitylcyclobutyl)-thiazolo [3,2-b][1,2,4]triazol-2-yl-phenol[e]	PVC membrane	Fluorescence	8.5×10^{-10} M	2 min
3-hydroxy-3-phenyl triaz-1-en-1-benzoic acid[f]	Agarose membrane	Absorbance	2.74×10^{-6} M	10 min

[a]Ensafi and Bakhshi (2003), [b]Shamsipur et al. (2004), [c]Amini et al. (2004), [d]Hashemi et al. (2011), [e]Aksuner et al. (2012), and [f]Rasolzadeh et al. (2019)

In this work, a commercial reagent, 4,7-diphenyl-1,10-phenanthroline-disulfonic acid disodium salt or bathophenantroline disulfonate (BPS) was used as a sensing reagent immobilized on a supporting material. BPS is known for its large molar absorptivity, 11,000 cm^{-1} M^{-1} at 535 nm (Hirayama et al., 2017). BPS is capable of complex formation, making it an excellent reagent for the spectrophotometric analysis of metals (Story, 1973). Sakamoto et al. (2016) introduced a straightforward method for visually quantifying total iron in human serum using BPS-loaded modified MCM-41. The quantification relies on observing the color intensity of the Fe^{2+}-BPS complex formed within the pores of modified MCM-41, which subsequently precipitates at the bottom of a well. The method exhibits a detection limit of 0.5 µM by discriminating the color intensity easily. However, the reuse of the sensing material was not reported. Therefore, it is necessary to develop and design an optical chemical sensor that can utilize BPS and allow for the reuse of the expensive sensing reagent, reducing chemical waste in the laboratory. Immobilization of the sensing reagent on a supporting material provides a viable alternative.

Figure 2.1 shows the structure of BPS. Nitrogen on the phenanthroline ring can interact with the nickel ion, quenching the BPS fluorescence signal. The reduction in the fluorescence signal can be correlated to the concentration of nickel ions. Additionally, BPS has two sulfonate groups that can be used to bind a supporting matrix modified with charged functional groups.
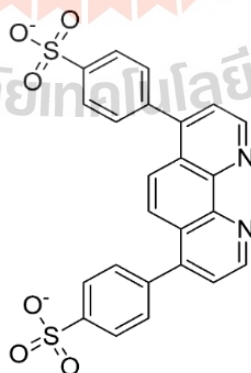
Figure 2.1 The chemical structure of bathophenantroline disulfonate.

2.3 Supporting materials

It is well known that choosing a suitable supporting material contributes to increasing the sensing performance. Many thin membranes are available and can be used to immobilize sensing reagents, such as acetyl cellulose (Ensafi and Bakhshi, 2003), Nafion (Amini et al., 2004), poly(vinyl chloride) (PVC) (Aksuner et al., 2012; Shamsipur et al., 2004), agarose (Hashemi et al., 2011; Rasolzadeh et al., 2019). In this work, mesoporous silica material was chosen as a supporting material. Mesoporous silica materials have pores with diameters between 2 and 50 nm, according to the International Union of Pure and Applied Chemistry (IUPAC) classification. Mesoporous silica materials have attracted great attention for several reasons: high surface area, porosity, tunable pore size, high silanol surface availability for modification with organic functional groups, and good chemical and thermal stability (Feng et al., 2013). Mesoporous silica materials can be synthesized using many methods and can provide a variety of morphologies, such as single crystals, spheres, rods, and fibers. However, the materials without support can be challenging to retrieve and reuse in sensing applications. As a result, the synthesis of mesoporous silica films (MSFs) onto glass substrates is an interesting alternative.

2.4 Synthesis methods of mesoporous silica film on a glass substrate

Several techniques are used for preparing MSF on glass substrates, such as the evaporation induced self-assembly (EISA) method, the Stöber solution growth method, and the electrochemically assisted self-assembly (EASA) method.

2.4.1 Evaporation induced self-assembly

Evaporation induced self-assembly is the method to synthesize MSFs via spin-coating or dip-coating techniques. The technique uses a homogeneous solution of a water-alcohol mixture, a silica precursor, and a surfactant template. Figure 2.2 shows the process of MSF formation on a substrate using the EISA methodology with the dip-coating technique. The film formation occurs when the substrate is pulled upward and

the solution is coated on the substrate surface. Polycondensation of the silica precursor forms silica around the surfactant template driven by solvent evaporation.

The EISA method can be used to create various pore structures, including 2D or 3D mesostructures, lamellar structures, or worm-like structures. However, the films produced by this method have randomly oriented mesochannels parallel to the substrate surface. Such pore orientation limits the accessibility and mass transport rate of molecules (Urbanova and Walcarius, 2014). One way to overcome this limitation is to synthesize MSFs with perpendicularly oriented mesochannels against the substrate surface. The pore orientation can improve the performance and response time of the sensor materials.
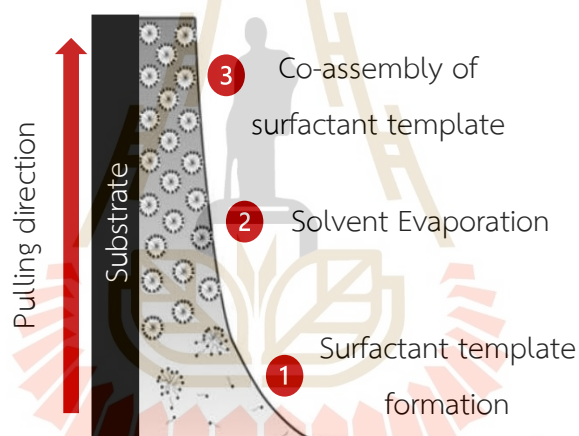
Figure 2.2 Illustration of the MSF formation process by dip-coating using the EASA method. Reprinted (adapted) with permission from Soler-Illia et al. (2010). Copyright 2010 Springer Science+Business Media, LLC.

The orientation of MSFs with perpendicular channels on the substrate surface can be synthesized using the Stöber solution growth method or the electrochemically assisted self-assembly method. The following section describes the syntheses and properties of MSFs based on these two methods.

2.4.2 Stöber solution growth

Teng et al. (2012) reported the first successful synthesis of uniform MSF with highly oriented and perpendicular mesochannels to the substrate surface by a Stöber solution growth method. In this method, MSF synthesis was achieved by immersing a substrate in a Stöber solution containing cetyltrimethylammonium bromide (CTAB) as a surfactant template, tetraethyl orthosilicate (TEOS) as a silica precursor, ethanol and ammonia under the quiescent condition at 60 °C. The formation of MSF proceeds through a gradual transformation of silicate-CTAB composites from spherical to perpendicular cylindrical micelles. This transformation relies on ammonia-catalyzed self-oriented growth at the solution-substrate interface and controlled silicate polymerization. The step of MSF formation using the Stöber solution growth method is described in Figure 2.3.
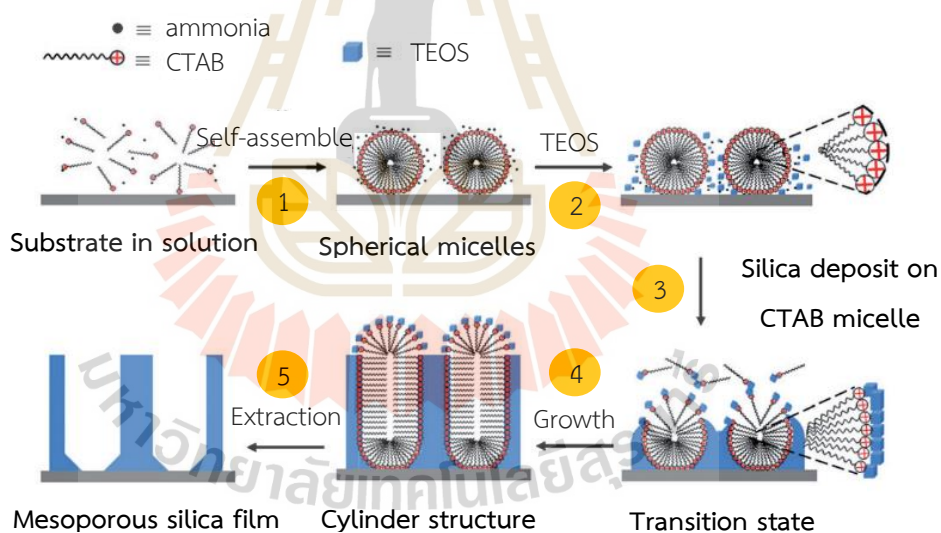
Figure 2.3 Illustration of the MSF formation process with perpendicular mesopore channels to the substrate using the Stöber solution growth method. Reprinted (adapted) with permission from Teng et al. (2012). Copyright 2012 Wiley-VCH Verlag GmbH & Co. KGaA, Weinheim.

Step 1: The surfactant cations (CTA$^+$) are adsorbed on a negative charge substrate, forming spherical CTAB micelle assemblies.

Step 2: The molecules of TEOS are slowly hydrolyzed in a controlled concentration of ammonia and ethanol solution to form negatively charged oligomeric silicate species that interact with the spherical micelle surface via electrostatic interaction.

Step 3: The free silica species are deposited at the junction between the spherical micelles and the substrate at a low concentration. Simultaneously, the ethanol diffuses into the CTAB micelles, causing a decrease in the interaction of the alkyl tail and an increase in the hydrophobic area of the micelles, leading to a lowering of micelle curvature.

Step 4: The ammonia is used to catalyze the growth of the MSFs and to promote the formation of hydrogen bonds between the surfactant template and the silicate oligomers, which also favors the transition from spherical to cylindrical micelles along with the longitudinal direction of cylindrical micelles that are perpendicularly oriented on the substrate.

Step 5: Calcination or solvent extraction is used to remove the surfactant from the mesopore channels.

In summary, the Stöber solution growth method provides the orientation of MSF with perpendicular channels on the substrate. This method is an attractive alternative in fabricating functional devices for sensor applications. The method is relatively simple and inexpensive, producing MSFs with good chemical and mechanical stability. However, the synthesis process takes a long time, 3-72 hours. Additionally, a new type of sandwich-like MSF has been synthesized with many mesochannel defects at a high reaction temperature (Teng et al., 2012). MSF synthesis methods with highly oriented and perpendicular mesochannels to the substrate under mild conditions and less synthetic time are interesting alternatives.

2.4.3 Electrochemically assisted self-assembly

Synthesis of MSF with highly oriented and perpendicular mesochannels to the surface under mild conditions and less synthetic time can be achieved using the EASA method. The principle of this method is to apply a suitable cathodic potential to a conductive substrate immersed in a sol mixture of silica precursor (TEOS) and surfactant template (CTAB) in a water/ethanol acid solution. After applying the potential, the reduction reaction of proton (H^+), water (H_2O), and nitrate (NO_3^-) generates hydroxide ions (OH^-) at the electrode surface. Hydroxide ion is a catalyst for the polycondensation of the sol, which leads to the formation of template silica mesopore channels that grow perpendicularly on the electrode surface, as shown in Figure 2.4. However, the film thickness synthesized using this method is in the range of 25-150 nm (Goux et al., 2009). The film thickness may be a limitation for sensor applications, as the thickness contributes to the surface area for the reaction and immobilization of the sensing reagents. Therefore, it is necessary to develop a method to overcome this limitation by increasing the film thickness.
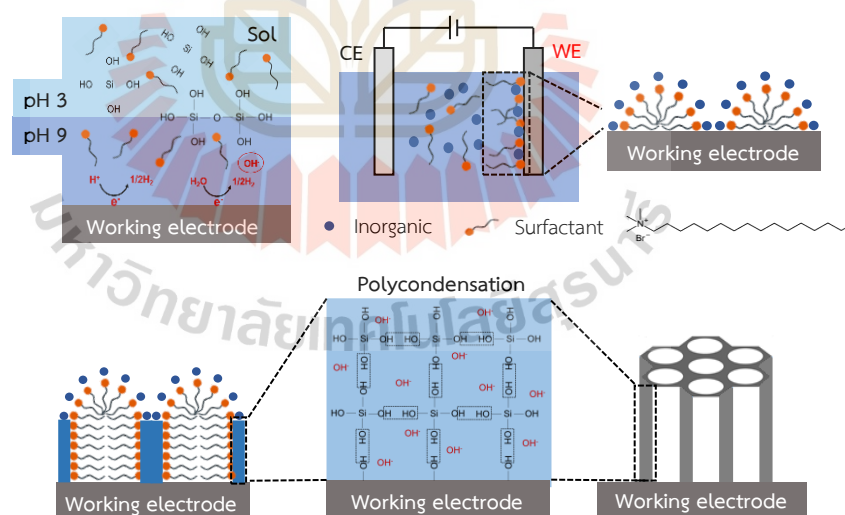
Figure 2.4 Illustration of the MSF formation process with perpendicular mesopore channels to the substrate using the EASA method. Reprinted (adapted) with permission from Walcarius (2015). Copyright 2015 Wiley-VCH Verlag GmbH & Co. KGaA, Weinheim.

The thickness of MSFs prepared by EASA can be controlled by adjusting the deposition time, current, applied potential, and precursor concentration. However, at high cathodic potentials and long deposition times, the hydroxide concentration on the electrode surface increases along with the diffusion layer. The situation leads to the competition between MSF formation and the deposition of unwanted silica particles on the MSF. Additionally, cracks may appear on the film upon drying due to the shrinkage effect (Ding and Su, 2015; Giordano et al., 2017).

Increasing the thickness of MSF without silica particles deposited on the film and crack-free films is achieved by sequentially applying the suitable potential to generate a multi-layered film (Giordano et al., 2017). In this method, the multi-layered film synthesis process was the same as that of single-layer MSF synthesis, but the potential is applied up to four consecutive times. For each cycle of potential application, the electrode is disconnected from the electrochemical cell and rinsed several times to prevent the polymerization of the silica precursors. The multi-layered film obtained from this method has highly ordered and vertically oriented mesoporous silica with thicknesses up to 400 nm. However, improving sensor performance is not solely reliant on increasing the MSF thickness. Silica surface modification and sensing reagent immobilization techniques also play a vital role in enhancing sensor performance.

2.5 Modification of mesoporous silica film with aminosilane

Silica materials have a high concentration of silanol (Si-OH) groups on their surface, which can be modified with organic functional groups to accommodate sensing reagent immobilization. In this research, 3-aminopropyltriethoxysilane (APTES) was used to modify the surface of MSF. APTES can covalently bond to silica via Si-O of APTES and Si-OH of the silica surface (de O. N. Ribeiro et al., 2019). Co-condensation and post-grafting are two methods used to modify the silica surface with amine functional groups.

2.5.1 Co-condensation

Co-condensation means incorporating the simultaneous condensation of silica and organosilane groups in the initial stage of the synthetic process of MSF, as shown in Figure 2.5. In this method, the organosilane groups are mainly embedded in the wall of the mesoporous silica framework, resulting in the homogeneous distribution of the organosilane groups over the mesopore and wall structure. However, the amount of organosilane added to the initial sol can affect the mesostructures.

Etienne et al. (2009) successfully prepared amine-functionalized oriented mesoporous silica films on the electrode. The level of functionalization was controlled by adjusting the APTES/TEOS molar ratios. The APTES content ranged from 0 to 20% mol (relative to the total mole of APTES combined TEOS). They found that the hexagonal mesostructures of oriented mesoporous silica films changed from ordered to disordered when the organosilane concentration in the sol was between 10 and 15%. In addition, increasing the percentage of APTES up to 15 or 20% resulted in a complete loss of the mesostructures. It was concluded that APTES up to 10% is sufficient to maintain the pore orientation mesostructures.

An increasing concentration of organosilane can lead to competition reactions between APTES and SiOH and adjacent APTES molecules, which can give rise to large APTES polysilane. As a result, there is a decrease in pore diameter, pore volume, and specific surface areas, which are known to be unfavorable to mass transport through the film (Hoffmann et al., 2006). Consequently, the amount of organosilane in co-condensation routes should be controlled appropriately.
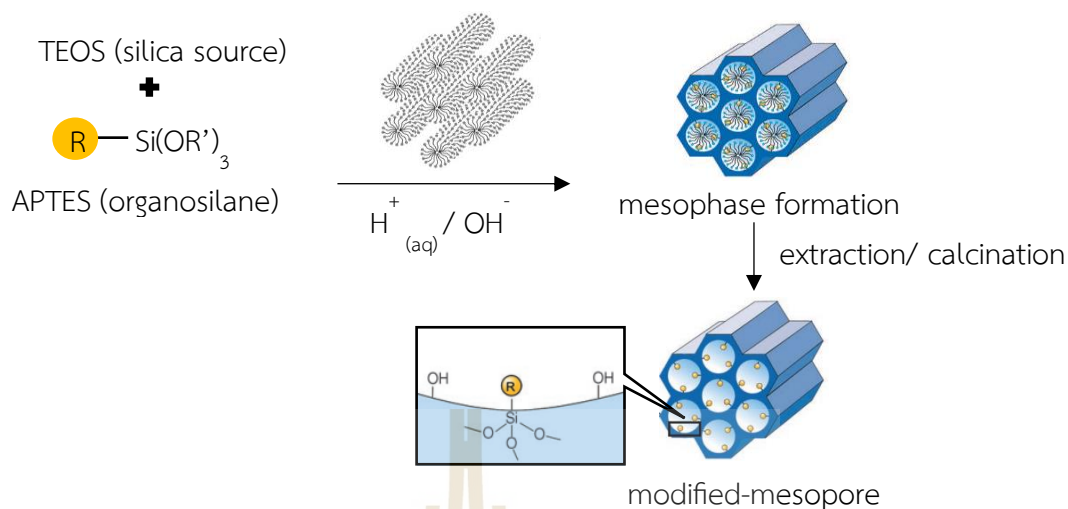
Figure 2.5 Illustration of the modification process of MSFs with the organosilane groups from APTES via the co-condensation route. Reprinted (adapted) with permission from Hoffmann et al. (2006). Copyright 2006 Wiley-VCH Verlag GmbH & Co. KGaA, Weinheim.

2.5.2 Post-grafting

Post-grafting refers to the modification of organosilane on the silica surface after the MSF synthetic and template removal process, as shown in Figure 2.6. The organosilane groups can form covalent or hydrogen bonds with the free silanol groups on the mesochannel surface. The post-grafting method provides more organosilane groups on the silica surface (Calvo et al., 2009; Feng et al., 2013). However, during the initial stages of the modification process, if the organosilane preferentially reacts at the pore openings, it can hinder the diffusion of other organosilane molecules into the pores. This results in an inhomogeneous distribution of organosilane groups on the silica surface and decreased pore size due to pore blocking (Hoffmann et al., 2006). Furthermore, the choice of solvent for dissolving the organosilane (anhydrous or aqueous solvents) and the method used for solvent removal also play a crucial role in the grafting process (de O. N. Ribeiro et al., 2019). Therefore, the design and development of synthesis conditions significantly impact the final silica product.

mesoporous pure silica   modified-mesopore structure
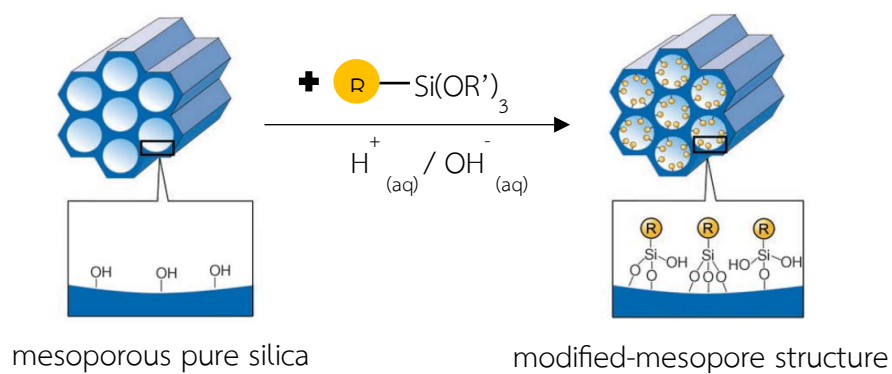
Figure 2.6 Illustration of the modification process of MSFs with the organosilane groups from APTES via the post-grafting route. Reprinted (adapted) with permission from Hoffmann et al. (2006). Copyright 2006 Wiley-VCH Verlag GmbH & Co. KGaA, Weinheim.
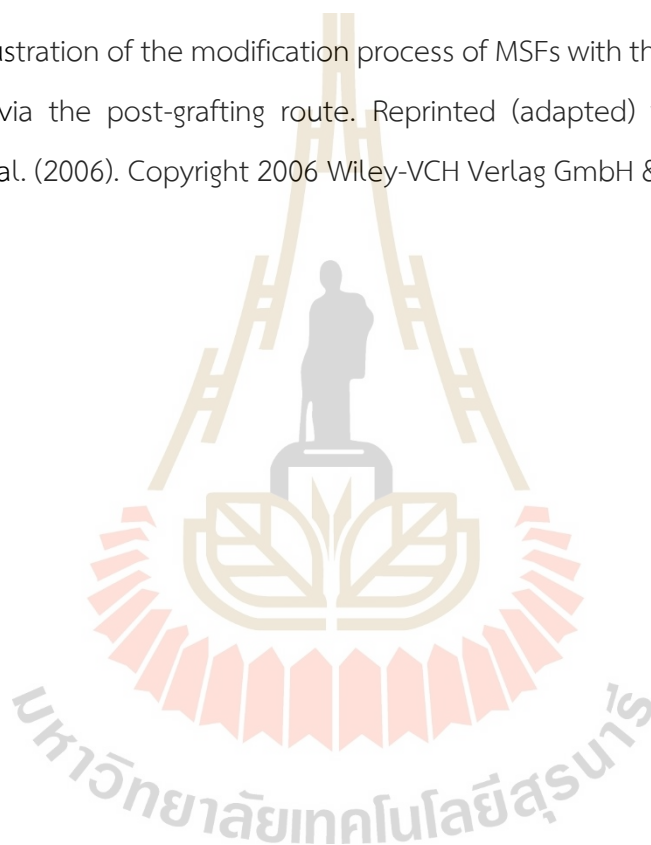
CHAPTER III

EXPERIMENTAL

3.1 Chemicals

The chemicals utilized in this research are listed in Table 3.1. All aqueous solutions were prepared using deionized (DI) water.

Table 3.1 Chemicals used in this research.

Chemicals	Formula	Content	Supplier
3-aminopropyltriethoxysilane (APTES)	$C_9H_{23}NO_3Si$	99%	Acros
acetone	CH_3COCH_3	99.8%	Carlo Erba
bathophenanthrolinedisulfonic acid	$C_{24}H_{14}N_2Na_2O_6S_2 \cdot 3H_2O$	98%	Acros
cetyltrimethylammonium bromide (CTAB)	$C_{19}H_{42}BrN$	99%+	Acros
citric acid anhydrous	$C_6H_8O_7$	99.5%	QRëC™
ethyl alcohol	C_2H_5OH	99.9%	Carlo Erba
ethylene diaminetetraacetic acid disodium salt, dihydrate	$C_{10}H_{14}N_2Na_2O_8 \cdot 2H_2O$	99%	QRëC™
hexaammineruthenium (III) chloride	$[Ru(NH_3)_6]Cl_3$	99%	Strem chemicals
hydrochloric acid	HCl	37%	RCI Labscan

Table 3.1 Chemicals used in this research (Continued).

Chemicals	Formula	Content	Supplier
Nafion®	$C_9HF_{17}O_5S$	~ 5% in a mixture of lower aliphatic alcohols and water	Sigma-Aldrich
nickel standard solution	$Ni(NO_3)_2 \cdot 6H_2O$	1,000 ppm	SpectrosoL, BDH
potassium hexacyanoferrate (III)	$K_3Fe(CN)_6$	99%	Merck
potassium hydrogen phthalate (KHP)	$C_8H_5KO_4$	99.9%	QRëC™
sodium citrate dihydrate	$C_6H_9Na_3O_9$	99%	BDH, AnalaR®
sodium hydroxide	NaOH	99%	Carlo Erba
sodium nitrate	$NaNO_3$	99%	Carlo Erba
tetraethyl orthosilicate (TEOS)	$Si(OC_2H_5)_4$	98%	Sigma-Aldrich
toluene	$C_6H_5CH_3$	99.8%	Carlo Erba

3.2 Apparatus and characterization

Electrodeposition and cyclic voltammetry experiments were carried out using a Palmsens EmStat[3+] potentiostat monitored by PSTrace software. The measurements were recorded in a three-electrode cell, including the mesoporous silica film-modified working electrode, an Ag/AgCl reference (ItalSens), and a mesh stainless steel counter electrode. Cyclic voltammetry was applied to characterize the film permeability using $Ru(NH_3)_6^{3+}$ or $Fe(CN)_6^{3-}$ as redox probes (at a concentration of 0.5 mM in 0.05 M KHP) and voltammograms were recorded at a scan rate of 100 mV s^{-1}.

Functional groups of synthesized films were identified by Fourier transform infrared spectroscopy (FTIR) on a Bruker Vertex 70 using attenuated total reflectance (ATR) mode with a resolution of 4 cm^{-1} and a number of scans at 64. The film morphology was characterized by scanning electron microscopy (SEM) and transmission electron microscopy (TEM). SEM images were taken using an Auriga Carl Zeiss microscope. Samples were sectioned with tile cut nippers and adhered on metal stubs with carbon tape. TEM images were obtained with a Talos F200X microscope at an acceleration voltage of 200 kV. Samples were scraped using a surgical blade and dispersed in ethanol. The samples were subsequently supported on carbon grids. The phases of the film were studied by X-ray diffraction (XRD). The experiments were performed at ambient temperature at Beamline 1.1W (Multiple X-ray Techniques) at Synchrotron Light Research Institute, Thailand, using the monochromatic synchrotron X-ray radiation of the energy 7.5 keV (wavelength of 1.66477 Å). Sample film was placed and aligned using a goniometer head. A diffraction pattern was recorded by a strip detector (Mythen6K 450, Dectris®) in the 2θ range of 0.9°–25° (with respect to the X-ray energy of 7.5 keV).

Fluorescence measurements were performed using a Perkin Elmer LS 50B spectrofluorometer with FL WinLab software. The excitation wavelength was 285 nm and emission spectra were recorded between 330 and 525 nm. The slit width for excitation and emission was 4.0 nm.

3.3 Preparation of mesoporous silica films

Mesoporous silica films (MSFs) were synthesized on fluorine-doped tin oxide (FTO) coated glass (surface resistivity ~7 Ω/sq, Sigma-Aldrich Pte Ltd) using an electro-assisted self-assembly (EASA) method, following the procedure described in the literature (Goux et al., 2009). The sol preparation and film deposition procedures were carried out at 20±2 °C. A typical sol mixture consisted of 20.0 mL of ethanol, 20.0 mL of 0.1 M NaNO$_3$ containing 1.0 mM HCl, 1.59 g CTAB, and 2.83 g TEOS; CTAB/TEOS ratio was 0.32. The final pH of the sol mixture was adjusted close to 3 by adding 0.1 M HCl. The mixture was aged for 2.5 h with stirring before use.

Before film application, an FTO glass was cleaned by sonication for 15 min in each following liquid, a detergent solution, acetone, ethanol, and DI water, respectively. The cleaned FTO glass was used as a working electrode (WE) in a three-electrode electrochemical cell, and the surface of the WE was limited to 0.8 x 1.5 cm using magic tape (3M, Scotch). Mesh stainless steel and silver/silver chloride (Ag/AgCl) electrodes were used as a counter electrode (CE) and a reference electrode (RE), respectively.

Three electrodes were immersed in the sol mixture, where the CE was placed about 1-2 mm from the WE. A potential of -1.3 V was applied for the desired time under quiescent conditions. The time for potential application of the 15 s or 30 s was set for synthesizing a single-layered film. The potential was applied sequentially up to four times to synthesize multi-layered films. For each cycle of the potential application, the WE was disconnected from the electrochemical cell and rinsed several times with DI water. The films were dried and aged overnight in an oven at 130 °C. The template was removed from the films by sonicating in an ethanol solution containing 0.1 M HCl for 15 min. This process was repeated twice.

3.4 Modification of MSFs with 3-aminopropyl triethoxysilane

MSFs were modified with APTES using the co-condensation and post-grafting methods. In the co-condensation method, the synthesis process was the same as that of MSFs described in section 3.3, except that APTES was added to the sol mixture. The sol mixture consisted of 12.24 mmol TEOS, 1.36 mmol APTES, and 4.35 mmol CTAB (Etienne et al., 2009). For the post-grafting method, MSF on FTO glass without surfactant was placed in a 1%v/v APTES in toluene under reflux conditions at 80±5 °C for 6 h (de O. N. Ribeiro et al., 2019). After refluxing, the modified MSFs were rinsed and sonicated with toluene to remove excess APTES. The films were dried at 60 °C for at least 24 h to remove the solvent. The modified films from the co-condensation and post-grafting route were denoted as $NH_2(C)$-MSF and $NH_2(G)$-MSF, respectively.

3.5 Immobilization of bathophenanthrolinedisulfonic acid on aminopropyl-modified MSFs

To immobilize BPS, aminopropyl-modified MSFs (NH_2-MSFs) were immersed in 0.1 M HCl for 1 h and then in DI water for 30 min to remove any excess acid. Next, the protonated NH_2-MSFs were soaked in 0.1 mM BPS solution for 18 h with stirring provided. Afterward, BPS-immobilized films were rinsed multiple times with DI water and dried at room temperature. When not in use, the obtained films were kept in a desiccator. BPS immobilized on NH_2-MSFs were designated as BPS/NH_2-MSFs.

3.6 Nafion coating on BPS/NH_2-MSF

Sensing films were coated with 1%w/v Nafion in ethanol. The sensing films were dipped in the Nafion solution for up to 3 cycles. In each cycle, the sensing films were dried at room temperature for 5 min before subsequent coating. Finally, the Nafion-coated BPS/NH_2-MSFs were dried in an oven at 60 °C for 24 h. The resulting Nafion-coated BPS/NH_2-MSFs were thoroughly washed with a copious amount of 0.01 M citrate buffer pH 6 to remove any unbound dye.

3.7 Response of sensing film to nickel ion and calibration study

A sensing film was immersed in a cuvette cell containing 2.5 mL of 0.01 M citrate buffer at pH 6.0 for 3 min. A nickel (Ni^{2+}) solution in citrate buffer pH 6.0 was added to the cuvette, and fluorescence signals were recorded for 60 min. All the above steps were carried out under stirring.

A calibration curve for Ni^{2+} was obtained by immersing the sensing film in Ni^{2+} solutions with different concentrations and monitoring the fluorescence signal at 395 nm under optimal measurement conditions.

3.8 Regeneration of sensing film

The multiple uses of a sensing film were investigated through regeneration using a suitable stripping reagent. After contact with a Ni^{2+} solution, a sensing film was soaked in a 0.1 M EDTA solution for a given time. It was then rinsed with DI water and immersed in a 0.01 M citrate buffer at pH 6 for 15 min. The fluorescence signal was recorded and compared with the initial signal of the sensing film.

3.9 Reproducibility

The reproducibility of the prepared sensing films from different batches was assessed. The signal measurements were made on the sensing films from eight batches of synthesized gel mixtures, five sensing films from each batch. The responses of the sensing films in the Ni^{2+} solution were also used for the evaluation. The reproducibility of sensing film response to Ni^{2+} was evaluated using three sensing films for signal measurement in the Ni^{2+} solution of the same concentration.

3.10 Interference study

The selectivity of the sensing film was evaluated through the interference study. Various ions, including Co^{2+}, Cu^{2+}, Mg^{2+}, and Zn^{2+}, were chosen for the study. Signal measurements were made with the sensing film in solutions containing only Ni^{2+} and Ni^{2+} with the studied ion at the optimum condition for Ni^{2+}.

3.11 Real sample analysis

Tap water samples were collected from equipment building 1 of Suranaree University of Technology in Nakhon Ratchasima, Thailand. The water samples were spiked with Ni^{2+}, and the pH of each sample was adjusted to 6.0 before analysis.
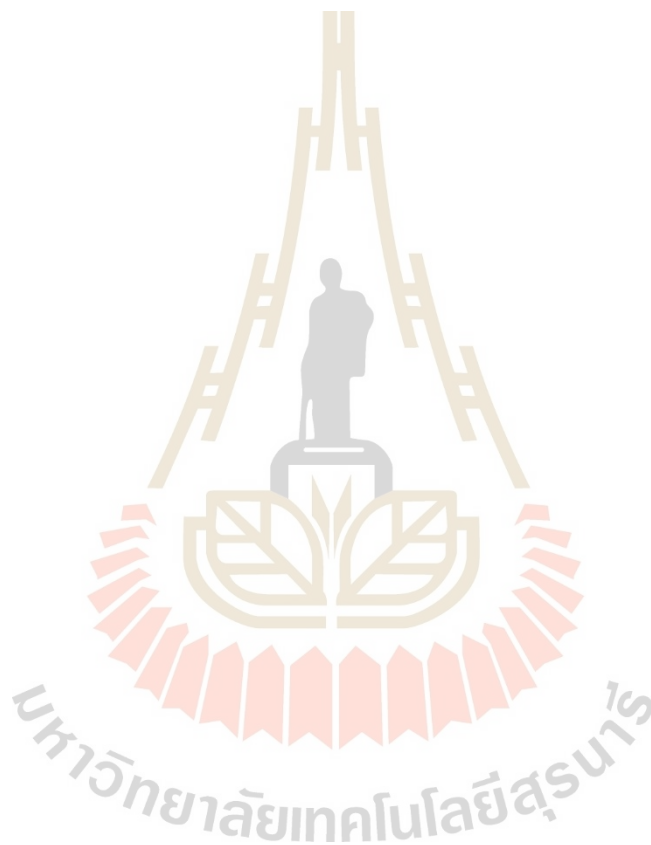
CHAPTER IV

RESULTS AND DISCUSSION

This chapter describes the development of an optical chemical sensor with a reusable sensing reagent. In this work, mesoporous silica films (MSFs) were used as a supporting material to immobilize 4,7-diphenyl-1,10-phenanthroline disulfonic acid disodium salt, also known as bathophenantroline disulfonate (BPS). The MSFs with various thicknesses were synthesized on FTO using electrochemically assisted self-assembly (EASA). The films were modified with 3-aminopropyl triethoxysilane to serve as a support material for immobilizing BPS and testing their ability to accommodate the dye. Several factors affecting BPS immobilization were investigated, including film thickness, amino modification method (co-condensation and post-grafting), pH, and BPS immobilization time. Finally, the BPS-immobilized MSFs were further studied as a potential optical chemical sensor for detecting nickel ion.

4.1 MSF synthesis using chronoamperometry

The chronoamperometry technique was utilized for the synthesis of MSF. A constant potential was applied on the electrode and the current was recorded against time. To obtain multi-layered films, the potential was applied sequentially (30 s/ layer). Figure 4.1(A) displays the current profiles recorded during the potential application. The current value was the highest in the synthesis of single-layered film, while it decreased with further deposition of the mesoporous silica layer on the FTO glass. The measured current resulted from the reduction of H^+, H_2O, and NO_3^- at the electrode surface to produce OH^- (Walcarius et al., 2007). A lower current was observed as the previously deposited silica layer with surfactant-templated hindered the diffusion of the electroactive species to the surface of the working electrode. Figure 4.1(B) presents

a photograph of FTO glass plates deposited with varying layers of MSF. As the number of layers of the film increased, the film appeared opaque.
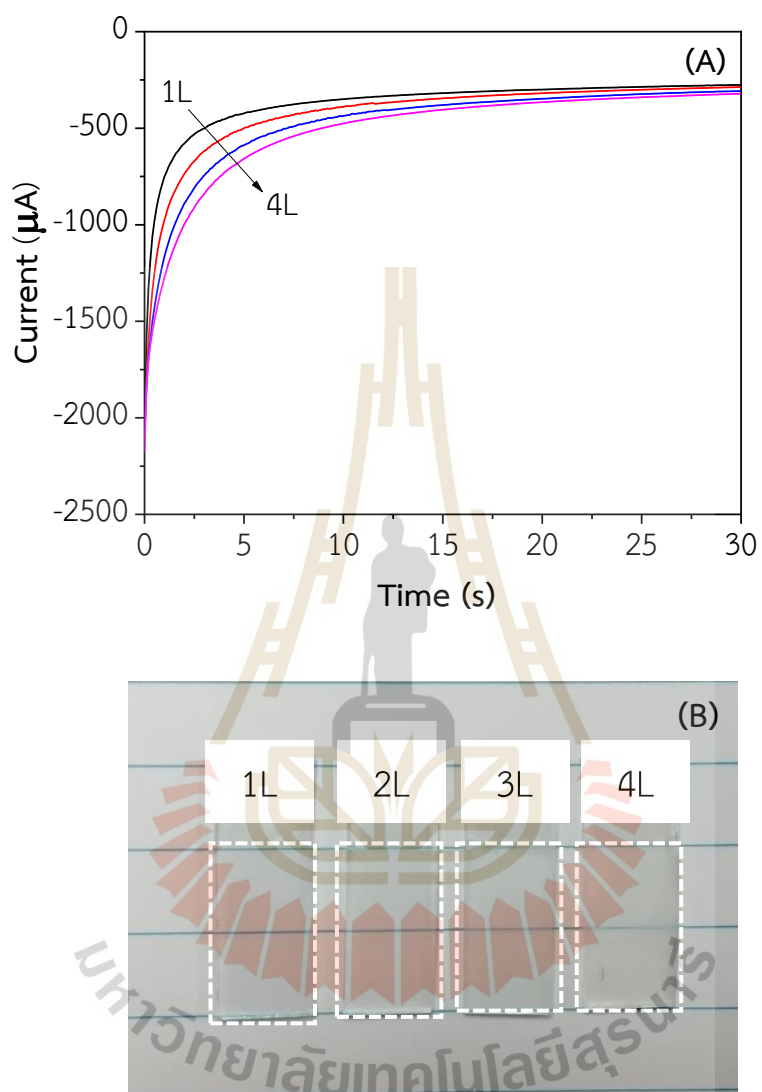
Figure 4.1 (A) Current profiles from the synthesis of MSF (B) A photograph of FTO glasses deposited with different layers of MSF. The symbols 1L, 2L, 3L, and 4L are the number of film layers deposited (30 s/ layer).

4.2 Characterization of MSFs

Cyclic voltammetry (CV) measurements were conducted to assess the quality and permeability properties of MSFs before and after CTAB extraction using a redox probe, $[Ru(NH_3)_6]Cl_3$ (cationic probe) and $K_3[Fe(CN)_6]$ (anionic probe) in solution. Half-reactions involving the two probes are shown in Appendix A. Voltammograms obtained from the studied in $[Ru(NH_3)_6]Cl_3$ solution and in $K_3[Fe(CN)_6]$ solution are shown in Figure 4.2 and Figure 4.3, respectively. For as-prepared films, the electrochemical responses of both redox probes disappeared when compared with the bare FTO, as shown in Figures 4.2(A) and 4.3(A). The results indicated that the silica film was coated onto the FTO glasses without cracks. The absence of current suggested that the probe species could not diffuse through the surfactant on the films to reach the electrode surface. After CTAB was removed from the films, the current response increased in the case of $Ru(NH_3)_6{}^{3+}$, as shown in Figure 4.2(B). The removal of CTAB opened up the pores on the film, and the probe molecules could diffuse through mesopore channels to interact with the electrode surface. Moreover, with an increase in the film thickness, the mass transport rate of the electroactive species could be lower, resulting in a lower current response in the thicker films. However, the current response was not observed when using $Fe(CN)_6{}^{3-}$ as shown in Figure 4.3(B), contributing from the negatively charged silica surface. Since the isoelectric point of silica is around 2-3, the silica surface is negatively charged in the potassium hydrogen phthalate solution, pH~4 (Ding et al., 2014).
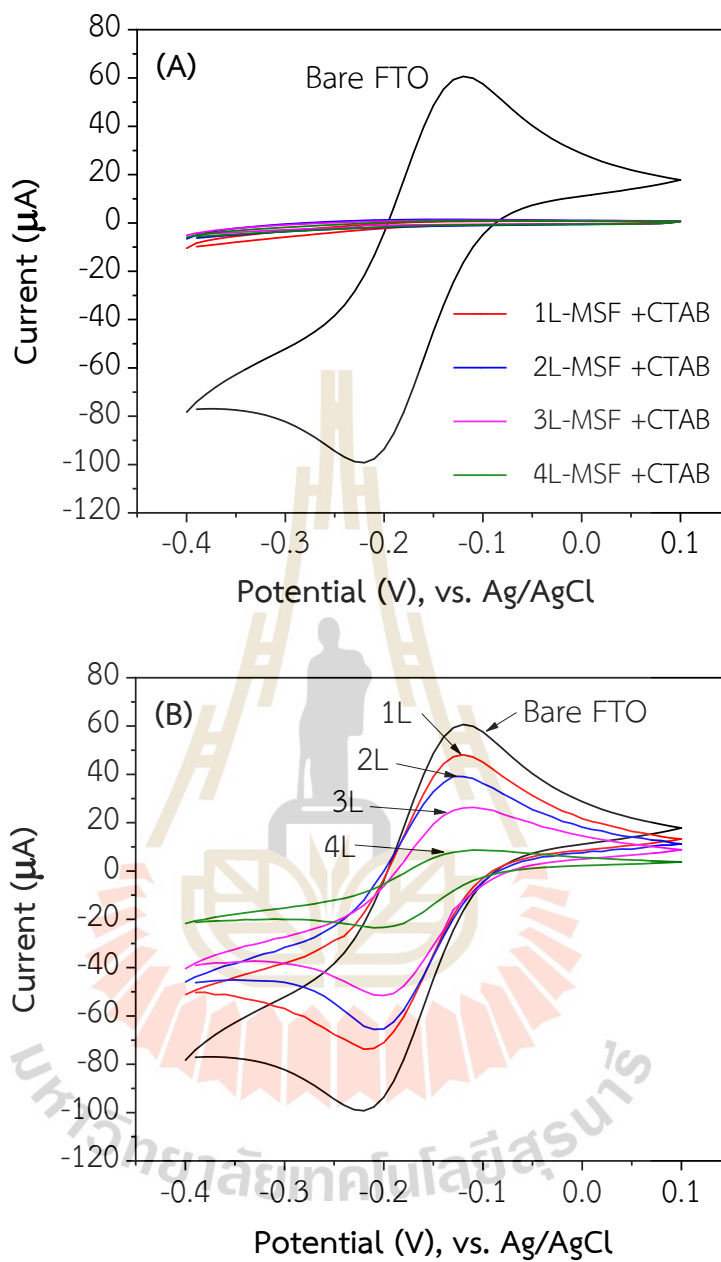
Figure 4.2 Cyclic voltammograms of multi-layered MSFs before (A) and after (B) CTAB removal recorded in 0.05 M KHP solutions containing 0.5 mM $[Ru(NH_3)_6]Cl_3$ at scan rate 100 mV s^{-1}.
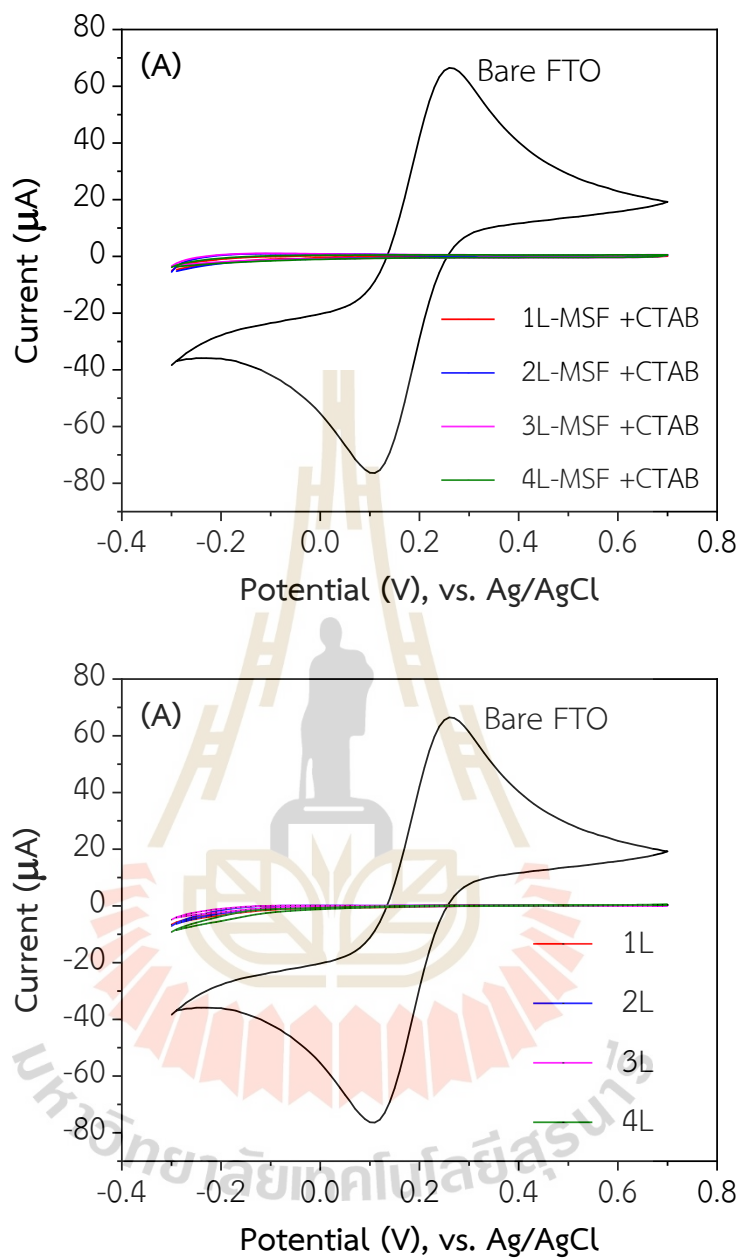
Figure 4.3 Cyclic voltammograms of multi-layered MSFs before (A) and after (B) CTAB removal recorded in 0.05 M KHP solutions containing 0.5 mM $K_3[Fe(CN)_6]$ at scan rate 100 mV s^{-1}.

The morphology of the multi-layered MSF was obtained using SEM and TEM, and the results are presented in Figure 4.4. The 1L, 2L, 3L, and 4L films were deposited on FTO-coated glass along with some silica particles, as shown in Figure 4.4(A-D). More silica particles are observed with more deposition layers. Furthermore, the cross-section FE-SEM images reveal film thickness in the 200-600 nm range, as shown in Figure 4.4(A′-D′).

TEM images show a well-ordered mesostructure with hexagonal packing, as shown in Figure 4.5 (A), and arrays of mesopore channels, as shown in Figure 4.5(B). The observed silica particle did not have a mesoporous structure, as shown in Figure 4.5(C).
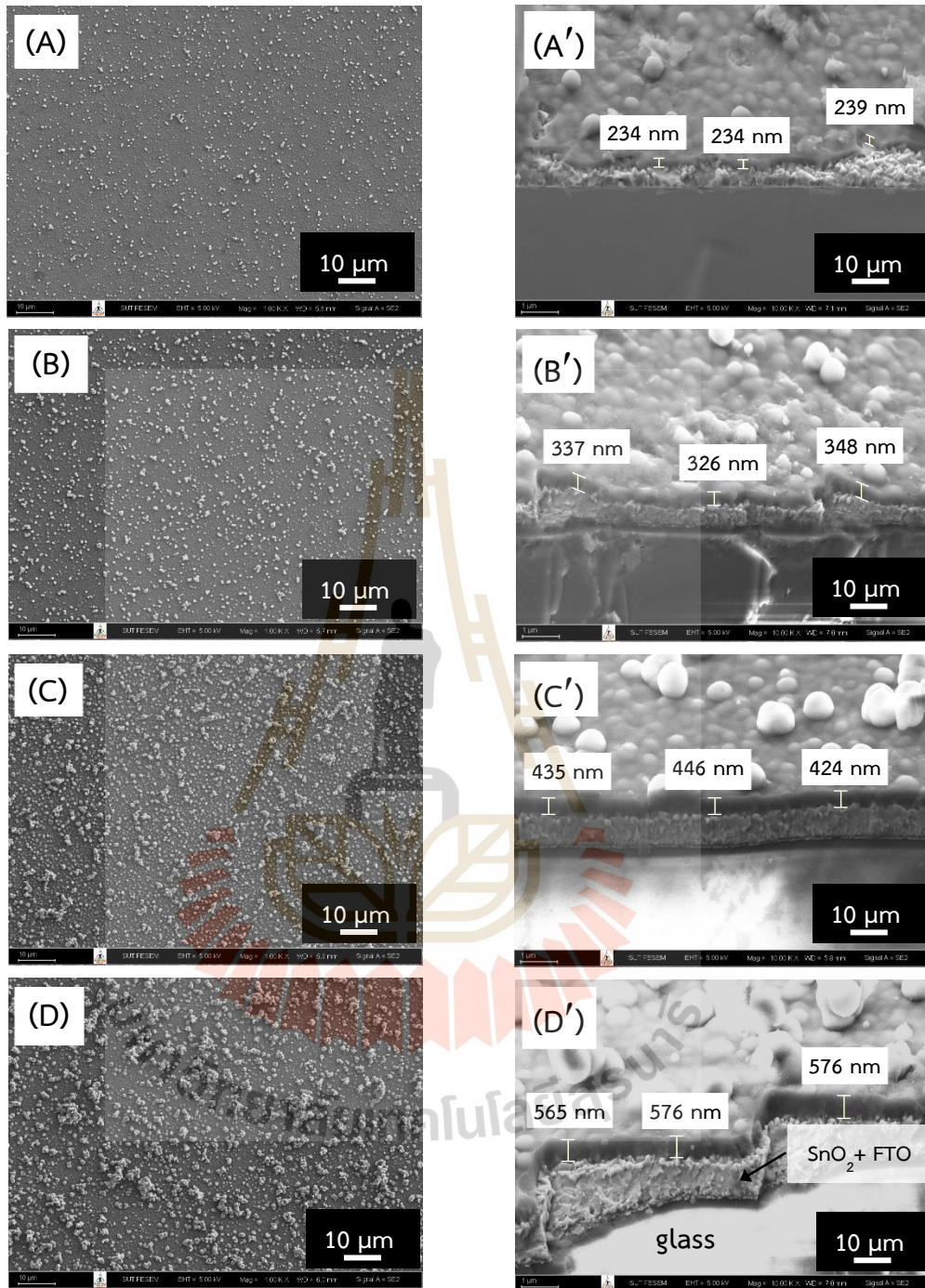
Figure 4.4 FE-SEM images of mesoporous silica film on FTO: (A-D) top view, (A′-D′) cross-section of 1L, 2L, 3L, and 4L-MSF.
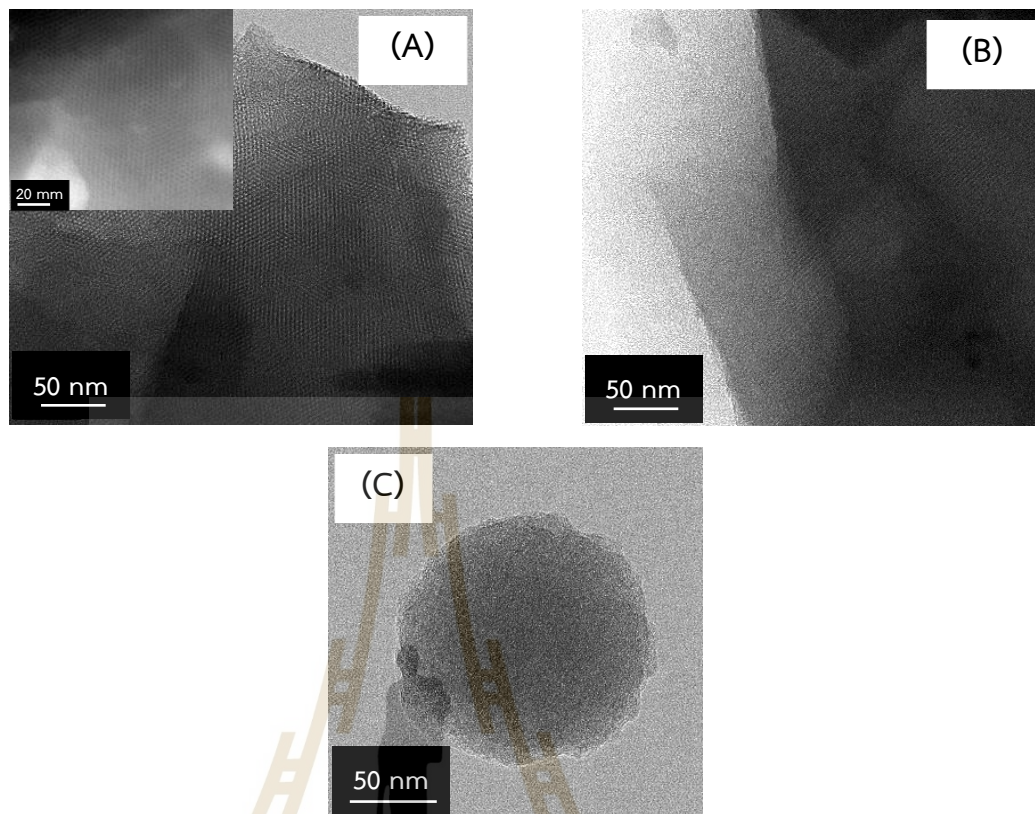
Figure 4.5 TEM images of 4L-MSF stripped from the FTO: (A) mesopores (B) arrays of mesopore channels, and (C) a silica particle.

The effectiveness of CTAB removal was assessed using FTIR spectroscopy. Fiure 4.6(A) shows the FTIR spectra of MSFs before CTAB removal, with bands at 2924 and 2853 cm^{-1} corresponding to the aliphatic -CH$_2$ chain of CTAB. Figure 4.6(B) shows the spectra in the absence of the two bands indicating that CTAB was removed from MSFs after ethanolic extraction. Furthermore, the FTIR spectrum of the parent silica exhibits characteristic vibration bands of the silica framework, including Si-O-Si asymmetric stretching at 1055-1070 cm^{-1}, Si-O-Si symmetric stretching at 803 cm^{-1}, and Si-OH stretching of silanol groups at 960-965 cm^{-1} (Etienne et al., 2009).
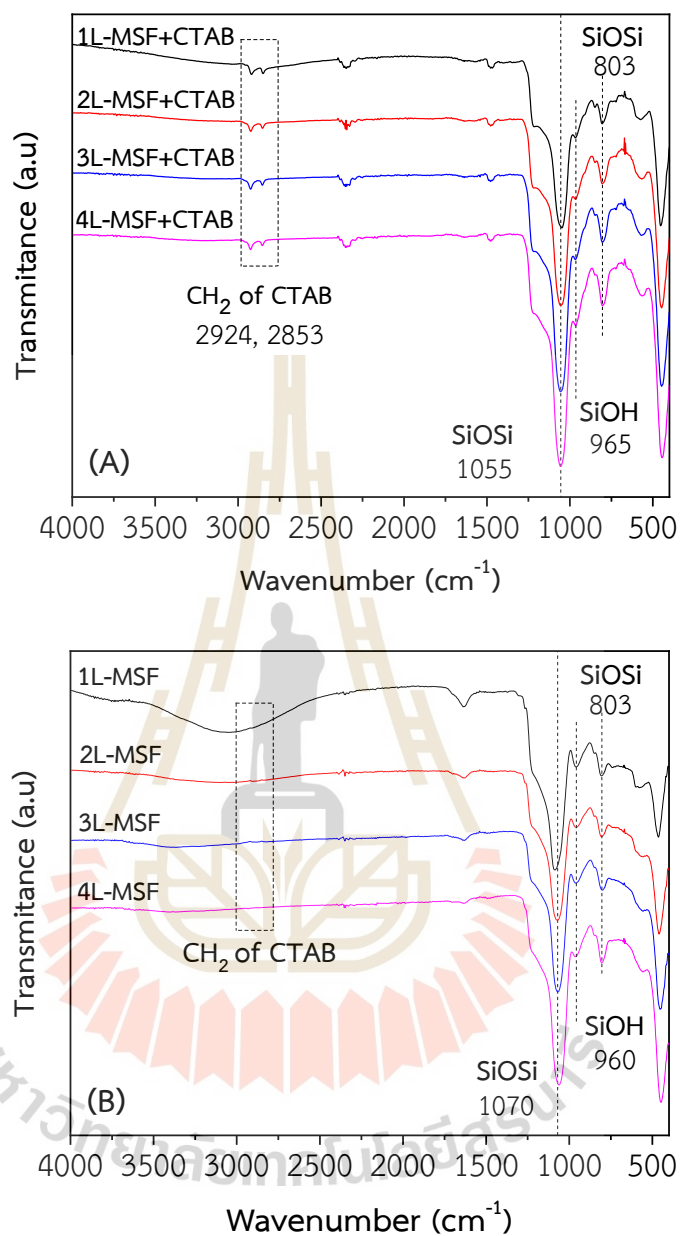
Figure 4.6 FTIR spectra of MSFs before (A) and after (B) CTAB removal.

XRD patterns of the films at low-angle are shown in Figure 4.7. A broad diffraction peak between 2.7° to 3.3° is attributed to the aggregated silica particles distributed over the film (Goux et al., 2009). Furthermore, the intensity increased and the peaks shifted to a lower angle in the presence of a larger amount of aggregated particles, and vice versa when fewer silica particles are present on the film, which agrees with SEM analysis in Figure 4.4.
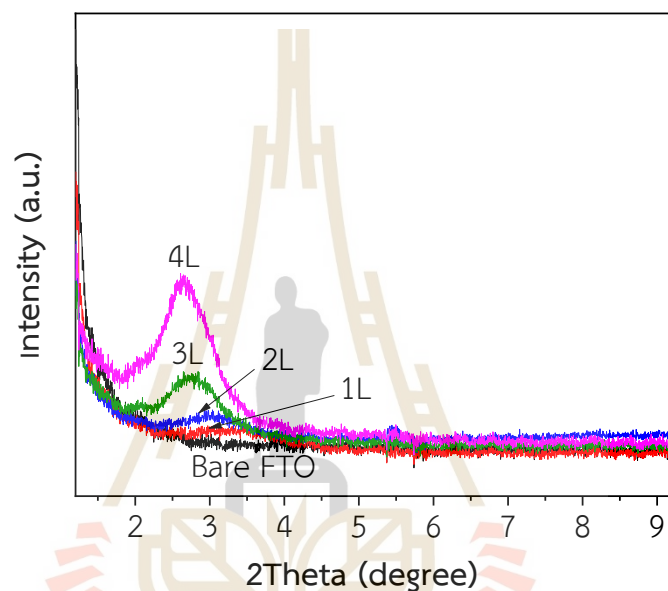
Figure 4.7 XRD patterns of MSFs on FTO glass.

4.3 Characterization of aminosilane grafting on MSFs

4.3.1 Electrochemical characterization of aminopropyl-modified MSFs from co-condensation and post-grafting route

Aminopropyl-modified MSF, designated as NH_2-MSF, synthesized from co-condensation, designated as NH_2-(C)-MSF, and post-grafting route, designated as NH_2-(G)-MSF with the concentration of aminopropyl ethoxy silane (APTES) of 1 %(v/v). The films were characterized using cyclic voltammetry with an anion electrochemical probe, $Fe(CN)_6^{3-}$. In Figures 4.8(A), 3L and 4L NH_2-(C)-MSF exhibited a current response to the probe only, whereas no current response was observed with 1L and 2L NH_2-(G)-MSF. The silica surface modification with the amine group should provide the positively charged MSF surface in a potassium hydrogen phthalate solution, favoring the anionic probe. Since the isoelectric point of silica is approximately 2-3, the silica surface becomes negatively charged in a potassium hydrogen phthalate solution, pH ~4 (Ding et al., 2014). For NH_2-MSFs from the co-condensation route, the current response increased with the thickness. This can be attributed to more aminopropyl groups on the silica wall from multi-layered deposits that could accumulate more $Fe(CN)_6^{3-}$ resulting in a higher current response for thicker films.

No current response was observed for NH_2-(G)-MSFs, as shown in Figure 4.8(B). In the post-grafting route, the amine precursor reacted at the pore entrance of the MSF could hinder the diffusion of other precursor molecules further into the pores, resulting in a nonhomogeneous distribution and a lower amount of the amine group within the pores (Hoffmann et al., 2006). Pore blocking is another possible explanation for the absence of a current response due to the relatively high amount of APTES used in the experiment (Talavera-Pech et al., 2016).

The permeability of NH_2-(C)-MSFs was significantly higher compared to that of NH_2-(G)-MSFs. This phenomenon could be from the different synthesis pathways. In the co-condensation route, the amine precursor was added during the initial stage of MSF synthesis. The amino groups are mainly embedded in the mesopore wall structure of the synthesized products, resulting in a homogeneous distribution throughout the mesopores and wall structure (Feng et al., 2013). As a result, probe species can permeate through the mesopores more effectively.
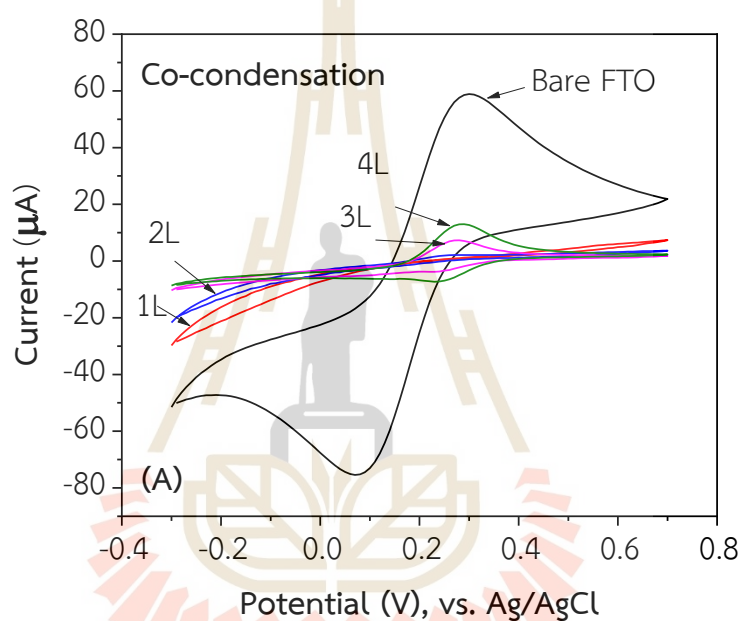
Figure 4.8 Cyclic voltammograms of modified NH_2-MSFs via co-condensation (A) and post-grafting route (B) recorded in 0.05 M KHP solution containing 0.5 mM $K_3[Fe(CN)_6]$ at scan rate 100 mV s^{-1}.
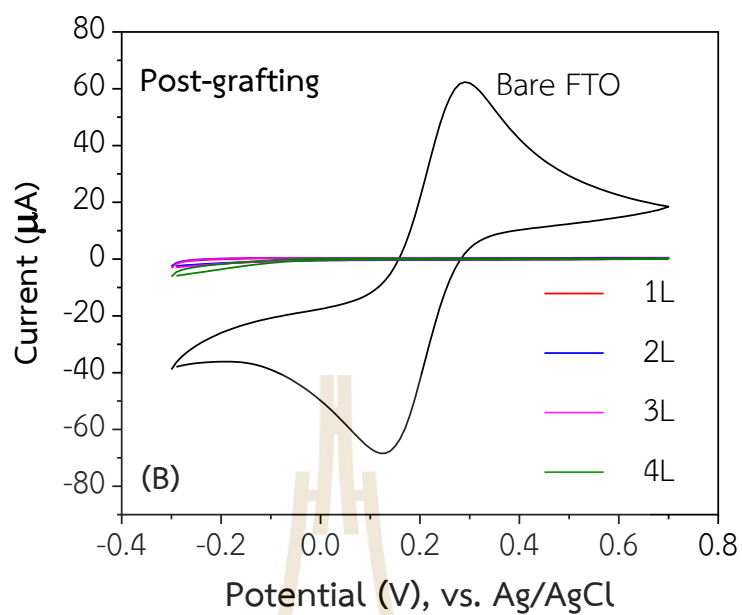
Figure 4.8 Cyclic voltammograms of modified NH_2-MSFs via co-condensation (A) and post-grafting route (B) recorded in 0.05 M KHP solution containing 0.5 mM $K_3[Fe(CN)_6]$ at scan rate 100 mV s^{-1} (continued).

4.3.2 Functional groups characterization of NH$_2$-MSF by FTIR

APTES grafting on the silica surface has been investigated using FTIR in attenuated total reflectance (ATR) mode. Figure 4.9 shows the FTIR spectra of 4L-MSF before and after grafting with 1% (v/v) APTES in toluene at 80 °C, 6 h. It can be observed that the band at 960 cm^{-1} corresponds to the disappearance of the free silanol (Si-OH), confirming the loss of the hydroxyl group after the attachment of APTES into the silica structure and the creation of a siloxane bond. The observation of a band attributed to the N-H group is obtained at 1621 cm^{-1}. The result indicates that APTES was successfully grafted onto the silica surface.
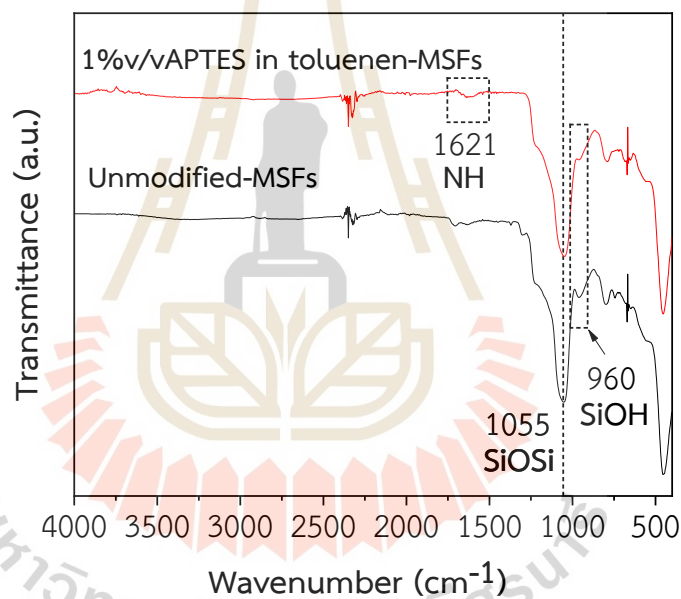
Figure 4.9 FTIR spectra of the MSF before and after amino modification by post-grafting method.

4.4 Characterization of sensing films

4.4.1 Effect of pH on BPS fluorescence

The influence of pH on BPS fluorescence intensity was studied by measuring fluorescence signals of 5.0 µM BPS solutions with controlled pH in the range of 3-6 using 0.01 M citrate buffer. The fluorescence intensity of the solution was measured at 395 nm. Figure 4.10(A) demonstrates that the fluorescence intensity increases with the increased solution pH from 3 to 6. The lower fluorescence intensity observed at lower pH values can be attributed to the protonated BPS. The protonation reduces the intensity at 395 nm and results in the appearance of another peak at 443 nm, as shown in Figure 4.10(B). Notice that there is an isosbestic point at 408 nm, suggesting the existence of two BPS species in equilibrium in the solution. Therefore, the BPS solution pH 6 was used in the study to keep BPS in the anionic form for immobilization on amino-modified MSFs.
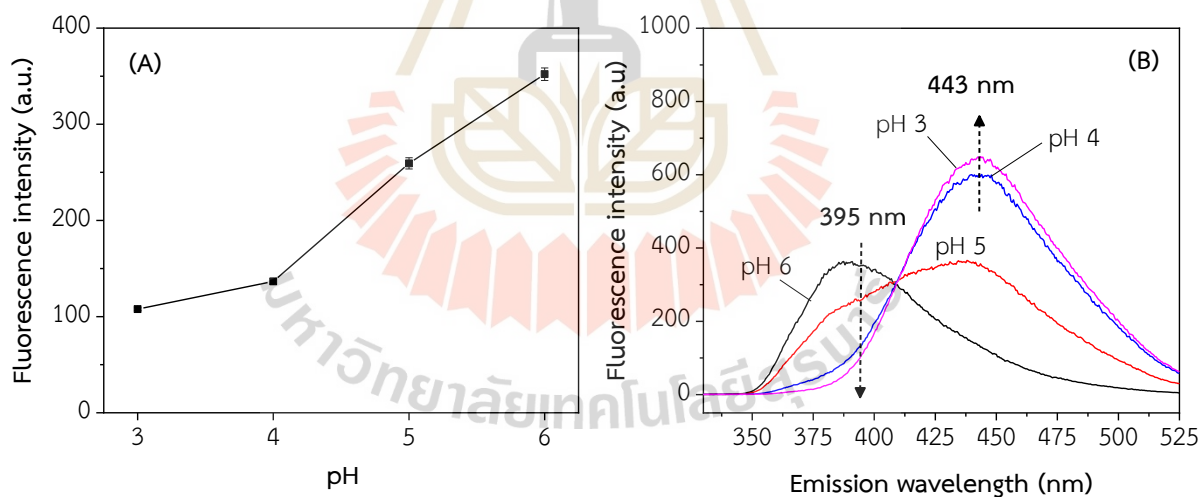
Figure 4.10 Fluorescence intensity (A) and spectra (B) of BPS in solutions at various pH. The solutions contained 0.05 mM BPS in 0.01M citrate buffer.

4.4.2 Fluorescence spectra of BPS-immobilized on NH$_2$-MSF from co-condensation and post-grafting route

Amino groups on the NH$_2$-MSFs were protonated before immobilizing BPS. The protonation resulted in positively charged amino groups on the films that could interact with the sulfonic groups (-SO$_3^-$) of BPS. BPS in an aqueous solution has an emission peak at 395 nm with an excitation wavelength of 285 nm, as shown in Figure 4.11. Figure 4.12 shows fluorescence spectra of BPS immobilized on NH$_2$-MSFs from co-condensation and post-grafting. BPS emission spectra were similar to that observed in the solution. The results indicate that BPS could be fixed on the NH$_2$-MSFs.

From the fluorescence spectra, the intensity obtained from NH$_2$-(G)-MSFs is higher than that obtained from NH$_2$-(C)-MSFs. The results suggested that more BPS was immobilized on NH$_2$-(G)-MSFs, implying the different nature of the modification route. Most amino groups are attached to the silica surface with various orientations in the post-grafting route. In contrast, the amino groups are incorporated into the silica wall with a vertical orientation in the co-condensation route (Hoffmann et al., 2006). As a result, the post-grafting films could have more amino groups available for dye immobilization than the co-condensation films. Additionally, the fluorescence intensity tends to increase with the number of layers. Therefore, the 4L-MSF obtained from the post-grafting route was selected for further study.
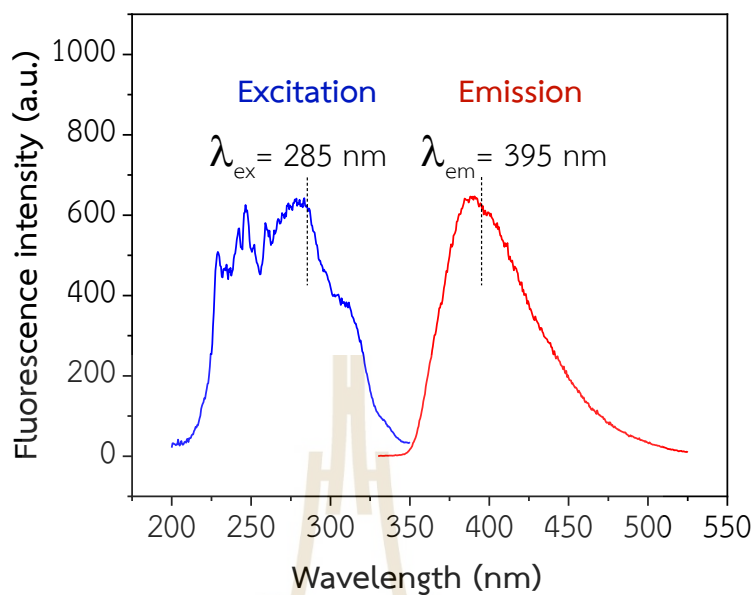
Figure 4.11 Fluorescence spectra of 0.02 mM M BPS solution.
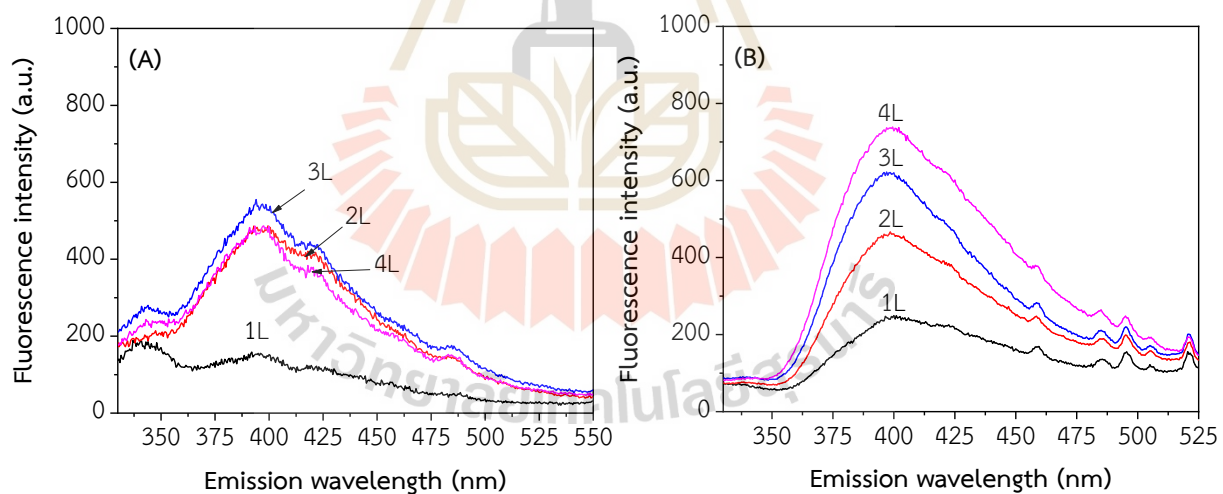
Figure 4.12 Fluorescence spectra of BPS on multi-layered NH_2-MSFs via co-condensation (A) and post-grafting route (B). The excitation wavelength was 285 nm.

4.4.3 Effect of time on dye immobilization

To study the effect of time on dye immobilization, aminopropyl-modified four-layered MSF, designated as 4L-NH$_2$-(G)-MSF, was immersed and stirred in 0.1 mM of BPS solution for 3 to 24 h. The fluorescence signal at 395 nm was then measured. The BPS immobilization time was varied to achieve the maximum fluorescence intensity. Figure 4.13 shows the emission spectra of immobilized BPS on 4L-NH$_2$(G)-MSFs, obtained after immobilization at different times. The fluorescence intensity increases with longer immobilization time. This study selected an immobilization time of 18 h, as the intensity of BPS on 4L-NH$_2$(G)-MSF should be sufficient to observe signal change in the presence of Ni^{2+}.
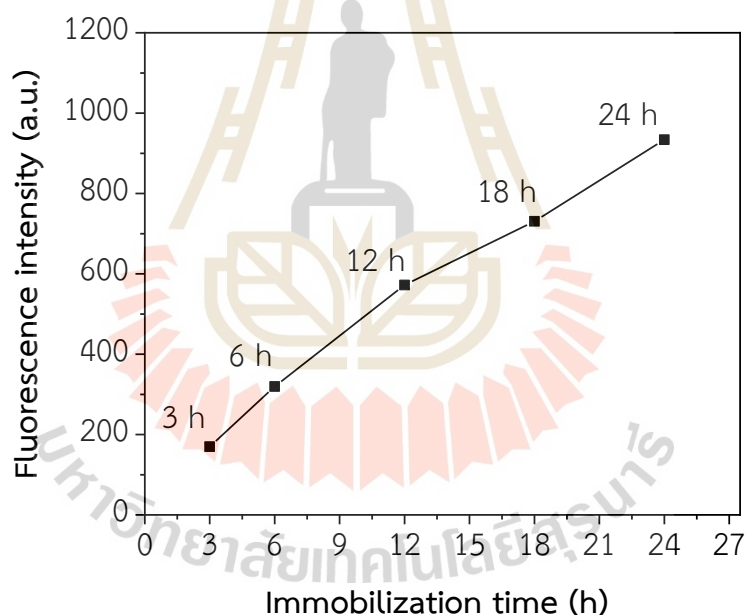
Figure 4.13 Fluorescence intensity of BPS on 4L-NH$_2$-MSF with different BPS immobilization time.

4.4.4 Reproducibility of sensing film preparation

The reproducibility of sensing film preparation was investigated by measuring the fluorescence signal of sensing films at 395 nm. Figure 4.14 show the fluorescence intensity of the sensing films prepared from eight batches of the sol-gel mixture and each batch consisted of five films. A relative standard deviation (RSD) of 8.79% was obtained from the measurements of all batches combined. The RSD values for each batch are also shown in Figure 4.14 . The results suggest that the film preparation was reproducible.
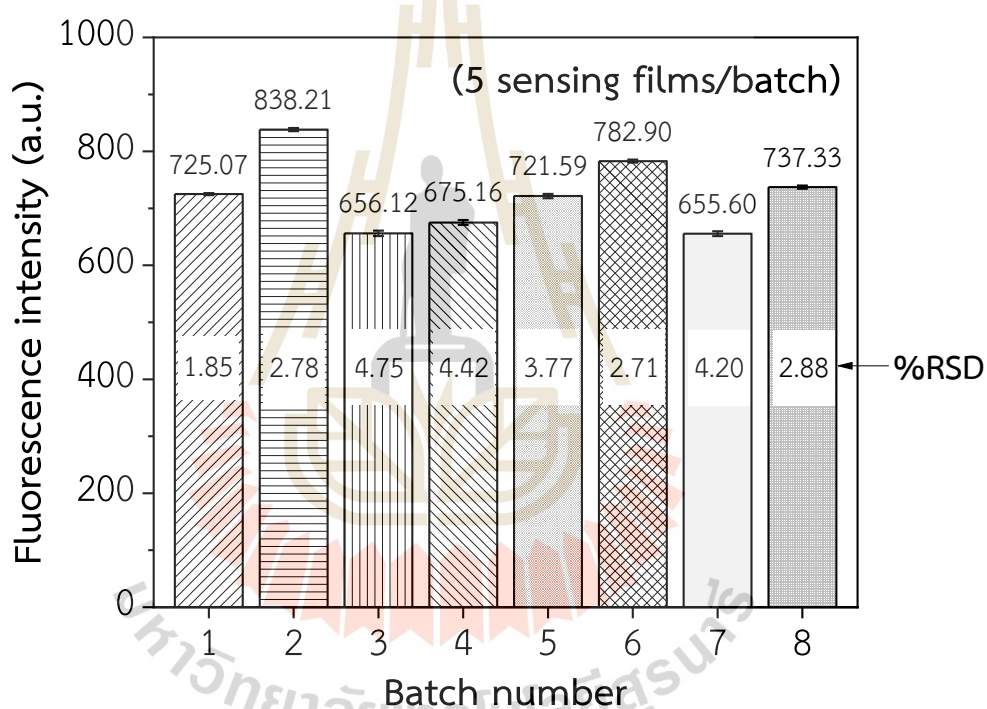
Figure 4.14 Fluorescence intensity at 395 nm of sensing films prepared of five sensing films from the different batches of the sol-gel mixture.

4.5 Response of sensing film to Ni^{2+}

4.5.1 Effect of pH on Ni^{2+}-BPS complex in solutions

The effect of pH on the nickel response to BPS in solution was studied before the study with the sensing films. A solution of 0.1 mM BPS in 0.01 M citrate buffer pH 6 was mixed with a solution containing 2.0 ppm Ni^{2+} at various pH values ranging from 3 to 6. After 30 seconds of mixing, the fluorescence intensity at 395 nm was measured. Figure 4.15 illustrates that the highest response (fluorescence quenching) was observed at pH 6.0. For solutions of pH value higher than 6 were not investigated due to the potential hydrolysis of Ni^{2+} ions, which would reduce the complexation between the metal ion and the reagent. Consequently, the solution pH 6.0 was deemed optimal and utilized for further studies with the proposed sensing film.
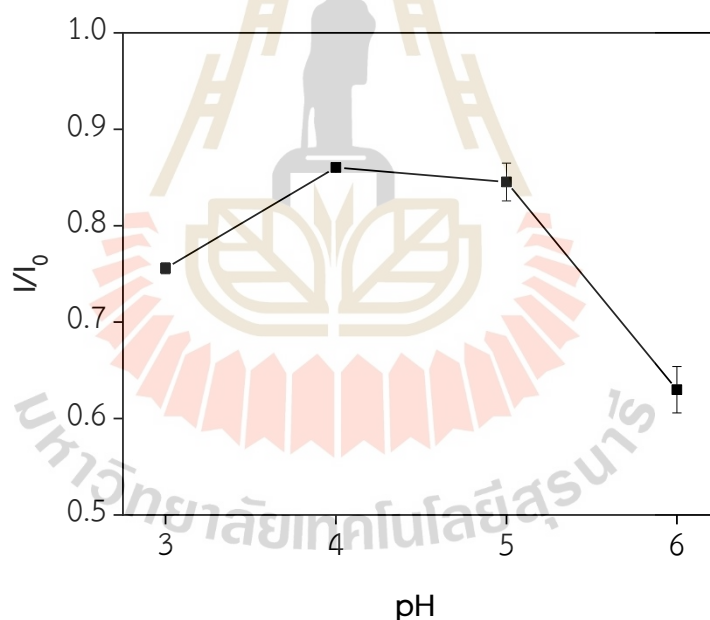
Figure 4.15 The effect of pH on the Ni^{2+}-BPS complex in solutions. The fluorescence measurements were made at 395 nm. The solutions contained 4.26×10^{-6} M Ni^{2+} at various pH in citrate buffer.

4.5.2 Response of sensing film to Ni^{2+}

The BPS-immobilized 4L-NH$_2$(G)-MSF was investigated for the detection of Ni^{2+} based on fluorescence quenching. The sensing film was conditioned in 0.01 M citrate buffer pH 6 for 15 min to obtain a stable signal, and then it was exposed to Ni^{2+} in 0.01 M citrate buffer pH 6. Figure 4.16(A) shows the fluorescence spectra of the sensing film before and after exposure to Ni^{2+}. Quenching of the fluorescence signal represents the interaction between the BPS and Ni^{2+}. This reduction in fluorescence signal can be attributed to different mechanisms, including collisional quenching, energy transfer, and chemical reactions (van de Weert et al., 2011). In the case of the Ni^{2+}-BPS, the fluorescence quenching of BPS could be from coordination bonds formed between the lone pair electrons of nitrogen in the phenanthroline ring of BPS and Ni^{2+} ions. This interaction could alter the excited state of BPS, leading to a decrease in its fluorescence intensity.

The sensing films were tested for their responses in Ni^{2+} solutions with a concentration from 0.1 to 20 ppm. The sensing film was conditioned in citrate buffer and then exposed to Ni^{2+} solution. The fluorescence signal at 395 nm was recorded every 2 s for 60 min. The response of the sensing film to Ni^{2+} was reported as the relative signal response, I_0-I/I_0, versus response time (s), where I_0 is the fluorescence signal at 395 nm after conditioning with 0.01 M citrate buffer for 15 min and I is the fluorescence signal at 395 nm after exposure to Ni^{2+} at different time intervals. Figure 4.16(B) demonstrated that the signal approached equilibrium in about 15 min. By measuring the relative fluorescence signal, one can determine the concentration of nickel ions present based on the degree of quenching observed.
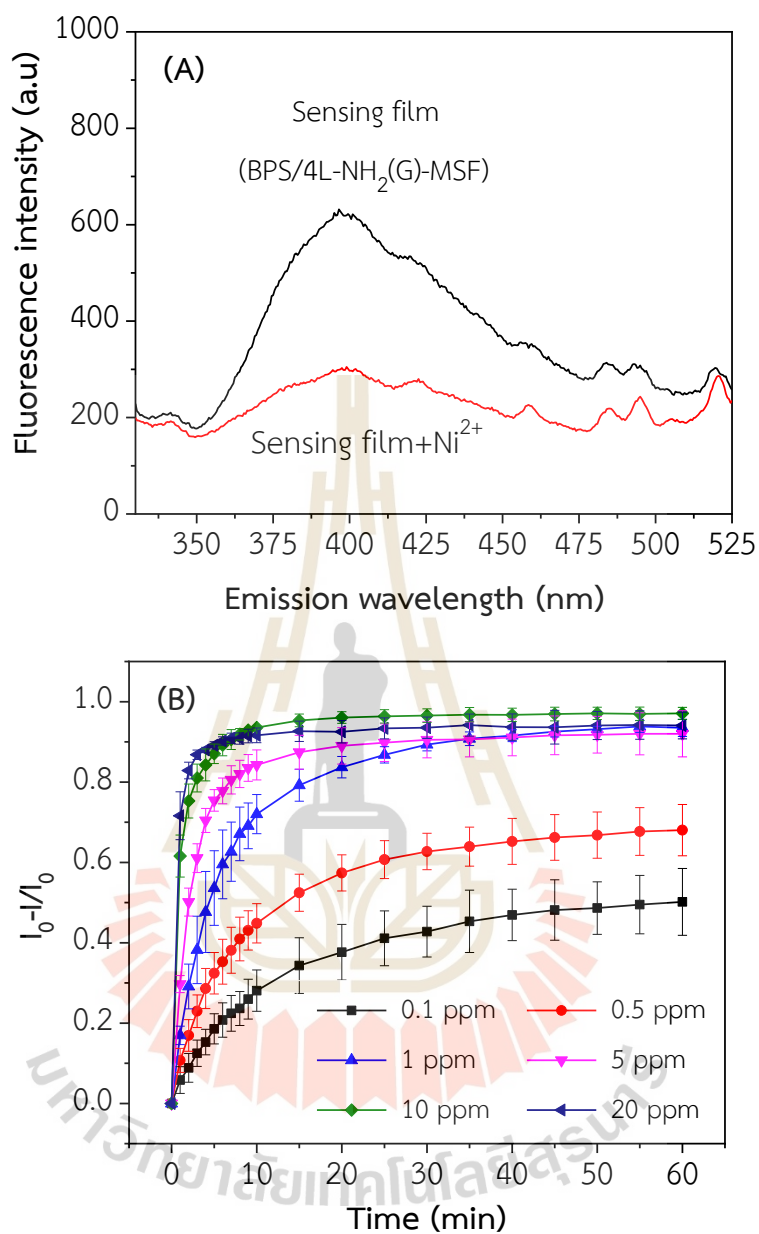
Figure 4.16 (A) Fluorescence emission spectra of a sensing film before and after exposure to 1.0 ppm Ni^{2+} (B) time profiles of response signals at 395 nm of the sensing films with different concentrations of Ni^{2+}. All experiments were performed in a 0.01 M citrate buffer pH 6.

Although the sensor can respond to Ni^{2+}, the high-water solubility of BPS (100 mg/mL) results in the leaching of BPS during the measurement. Figure 4.17 shows an emission spectrum of BPS leached into a Ni^{2+} solution after the measurement in the 0.1 ppm Ni^{2+} solution. It is possible that the reduction in fluorescence signal during the response to Ni^{2+} occurs due to a combination reaction between Ni^{2+} and BPS on the sensing film, as well as in the solution. Consequently, improving the sensing films to reduce reagent leaching is critical for enhancing the accuracy and reliability of the analysis.
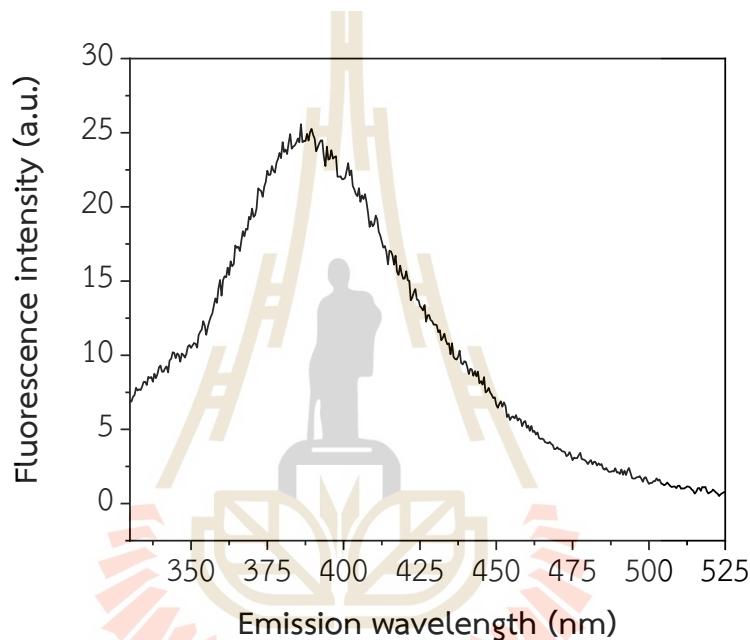
Figure 4.17 Fluorescence emission spectra of BPS leached into Ni^{2+} solution after removing the sensing film from the solution.

4.6 Development of Nafion-coated sensing film

The previous experimental results revealed that BPS leached out in the aqueous solutions. Therefore, an effort to reduce BPS leaching was investigated by coating the sensing film with Nafion. Nafion is a polymer with hydrophobic and hydrophilic structures, as shown in Figure 4.18. These properties provide suitable conditions for trapping the sensing reagent, while the sulfonate groups provide ion exchange. Nafion coatings have been extensively studied and developed for sensor applications due to their good chemical, thermal, and mechanical stability and high transparency, making them suitable for optical chemical sensors (Amini et al., 2004).
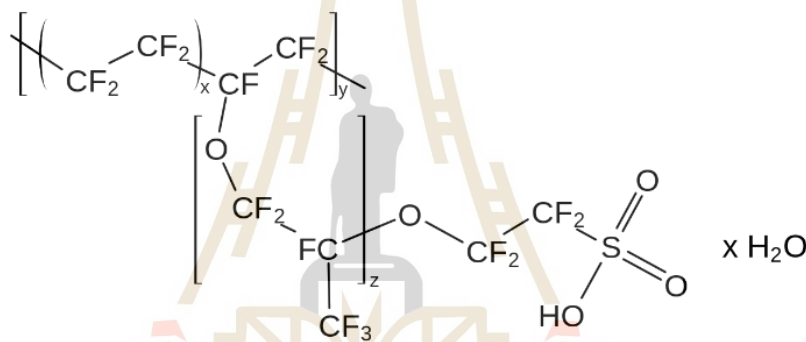
Figure 4.18 The structure of Nafion.

In the previous experiment, sensing films were prepared by synthesizing multi-layered MSF with a 30 seconds/ layer deposition time of up to four consecutive times to increase the film thickness. However, the SEM results revealed that the synthesized films had silica particles starting from the first layer (1L) of film synthesis. The formation of silica particles could partially block the active electrode surface and lower the amounts of produced OH$^-$ catalyst at the interface (Giordano et al., 2017), and consequently, slower film growth with unwanted silica particles over the film. Too long a deposition time was the cause for silica particles to form at the interface. As the film thickness increased with the number of film layers, the likelihood of the silica particles blocking the film pores would increase continuously. Based on the experimental

results, deposition time was reduced to 15 seconds/layer for preparing MSFs for sensing film development.

4.7 MSF synthesis with reduced deposition time

The chronoamperometry technique was used to synthesize multi-layer MSF with a potential step of -1.3 V for 15 seconds. Figure 4.19 shows the current profile of MSF synthesis. The current profiles in the synthesis of the first and second layers are similar, indicating that the generation of OH^- from the reduction reaction of H^+, H_2O, and NO_3^- on the surface of the electrode occurs simultaneously with film formation. However, the current profile of the third layer synthesis appeared different with lower current values. The results suggested that simultaneous silica particle formation along with the MSF synthesis process could hinder the diffusion of the electroactive species to the surface of the working electrode.
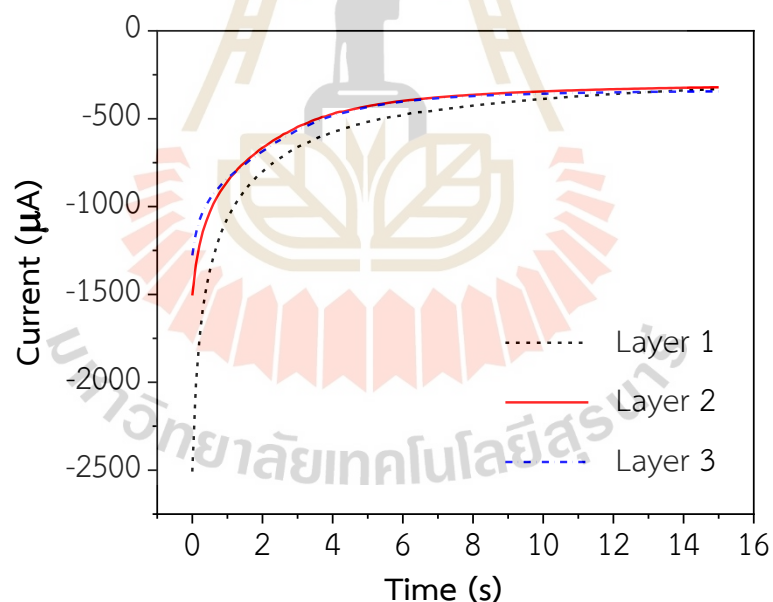
Figure 4.19 Current profiles from the synthesis of MSF with a deposition time of 15 seconds/layer).

4.8 Characterization of MSF synthesized with reduced deposition time

The as-synthesized MSFs were characterized using cyclic voltammetry to study their permeability and uniformity. The MSFs before and after CTAB removal were investigated using cationic electrochemical probes, $[Ru(NH_3)_6]Cl_3$. Figures 4.20(A) and 4.20(B) show the cyclic voltammograms of the MSFs before and after CTAB removal, respectively. For as-prepared films, the film synthesized using 15 seconds of deposition time exhibited a slight current signal indicating that the film might not be uniformly covered on the FTO glass. No current signal was observed when the number of layers was increased to two or three. The results suggested that MSF synthesis starting from two layers could be achieved on FTO glass without cracks. Giordano et al. (2017) reported that 15 seconds is the minimum deposition time required to obtain a uniformly covered MSF without cracks. They found that films with a deposition time of less than 15 s had an uneven appearance, and no film was formed if the synthesis time was less than 10 seconds.

After CTAB removal from the films, current signals were observed due to the electroactive species being able to move through the opened nanopores and undergo reactions on the surface of the electrode. The current signal of the 1L (15 seconds) synthesized film is almost comparable to the signal of the bare FTO. This is expected to be the result of reducing the synthesis time of the film, which reduces the occurrence of silica blockage particles, allowing for good accessibility of the substance through the opened pores. When considering the current signals of the 2L (15/15 seconds) and 3L (15/15/15 seconds) films, it was found that the current signal of the 2L film slightly decreased. This is due to the mass transport resistance at different film thicknesses.
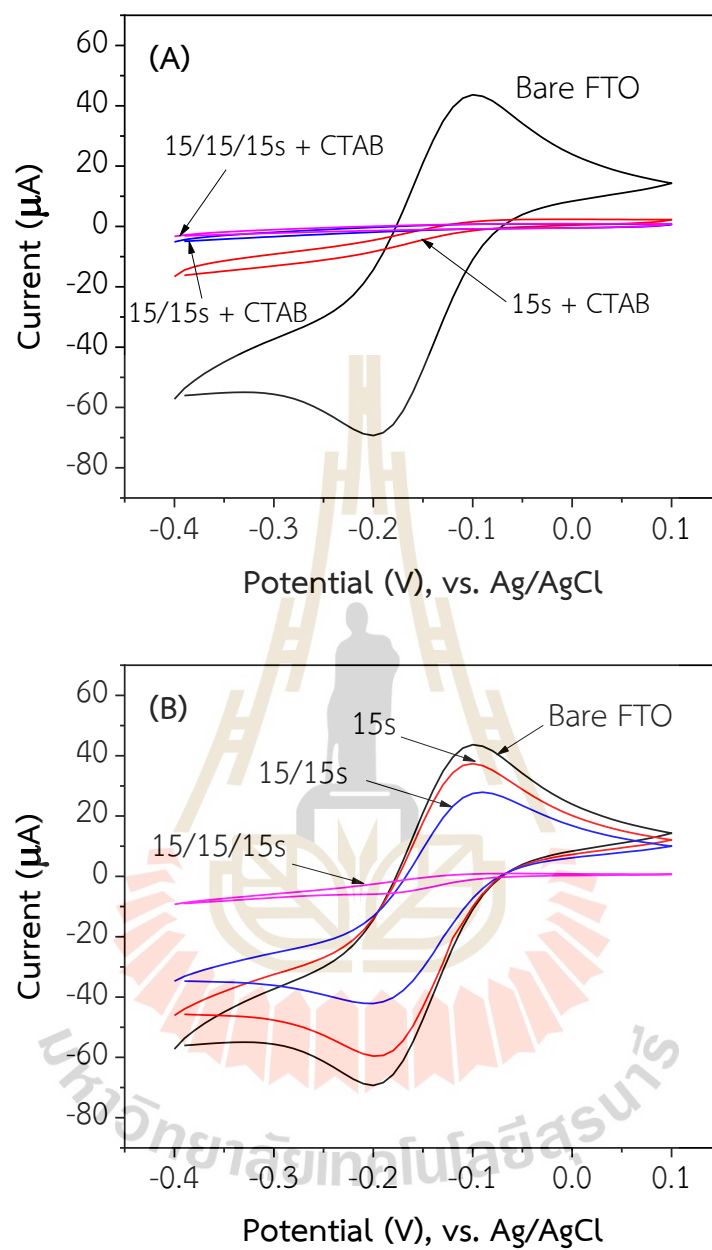
Figure 4.20 Cyclic voltammograms of MSFs before (A) and after (B) CTAB removal recorded in 0.05 M KHP solutions containing 0.5 mM $[Ru(NH_3)_6]Cl_3$ at scan rate 100 mV s^{-1}.

The morphology of the MSFs synthesized with a deposition time of 15 seconds per layer was characterized using SEM, and the results are presented in Figure 4.21. The films prepared with 1L (15 s), 2L (15/15 s), and 3L (15/15/15 s) were coated on FTO glass and appeared as thin films, as seen in Figures 4.21 A, B, and C, respectively. In addition, reducing the deposition time of film synthesis contributed to decreasing the amount of silica particles over the thin film. However, the amount of silica particles increased as the number of film layers increased. This is evident in the 15/15/15 s synthesized film. Furthermore, the cross-sectional FE-SEM images of the films exhibited a thickness in the range of 100-150 nanometers, as seen in Figures 4.21 A′, B′, and C′. Based on the experimental results from CV and SEM, the 2L-MSF was selected for sensing film fabrication, as it exhibited good accessibility with a uniform film and a small amount of silica particles on the film.
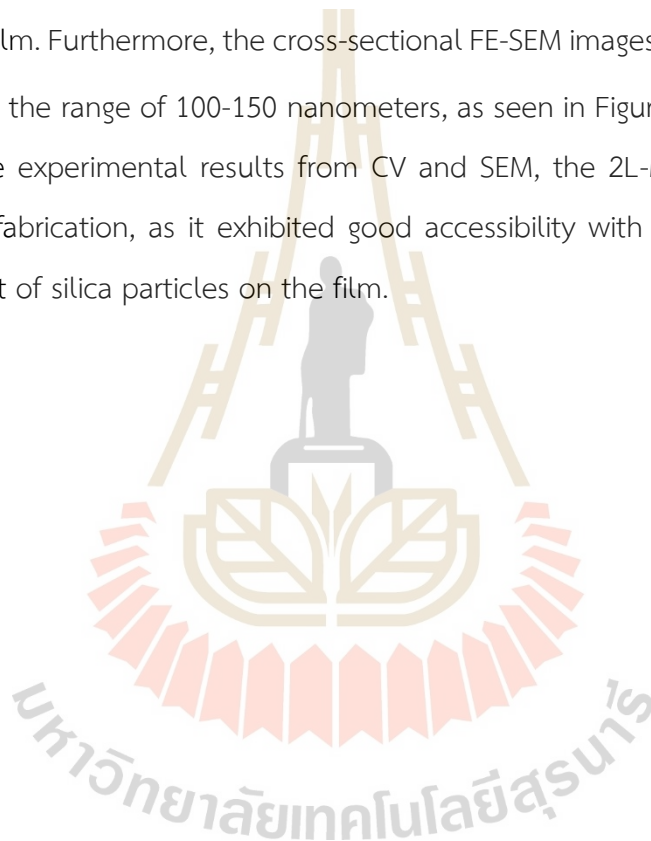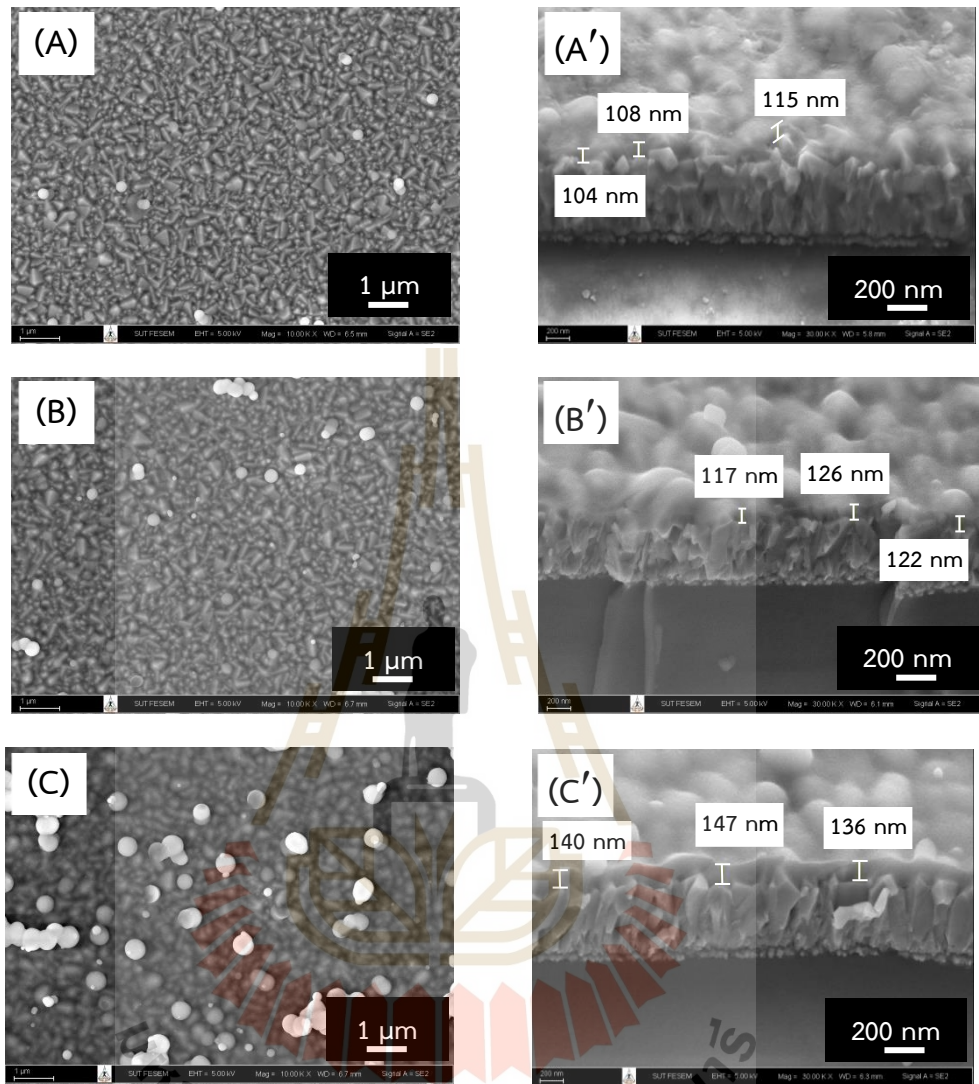
Figure 4.21 FE-SEM images of mesoporous silica film on FTO: (A-C) top view, (A′-C′) cross-section of 1L, 2L, and 3L synthesized with deposition time of 15 seconds/layer.

4.9 Characterization of Nafion-coated BPS-NH$_2$-MSF

4.9.1 Fluorescence spectra of Nafion-coated BPS-NH$_2$-MSF

The 2L-MSFs were chosen to modify with APTES using the post-grafting method. The films with CTAB removed were refluxed in a 1% (v/v) APTES in toluene at 80 ℃ for 6 h. Then, the obtained films were protonated in 0.1 M HCl for 1 h and immobilized with BPS by immersing in 0.1 mM BPS solution at 20 ℃ for 18 h. Finally, the BPS-immobilized-MSFs were coated with Nafion to prevent dye leaching.

The films after coating with Nafion was characterized by fluorescence technique. The fluorescence spectrum of the Nafion-coated BPS-NH$_2$-MSF exhibited an emission peak at 415 nm, as shown in Figure 4.22(A). The Nafion-coated BPS-NH$_2$-MSF has a slight difference in the emission spectrum compared with BPS-NH$_2$-MSF (without Nafion coating). However, after the Nafion-coated film was soaked in 0.1 M citrate buffer pH 6, the obtained spectrum appeared the same as the film without coating. In addition, when measuring the buffer solution after removing the Nafion-coated film, the fluorescence spectrum of BPS was observed, as shown in Figure 4.22(B). This is expected to be from excess BPS on the Nafion layer. Therefore, removing the excess BPS is crucial to ensure no BPS release during sensor response studies.
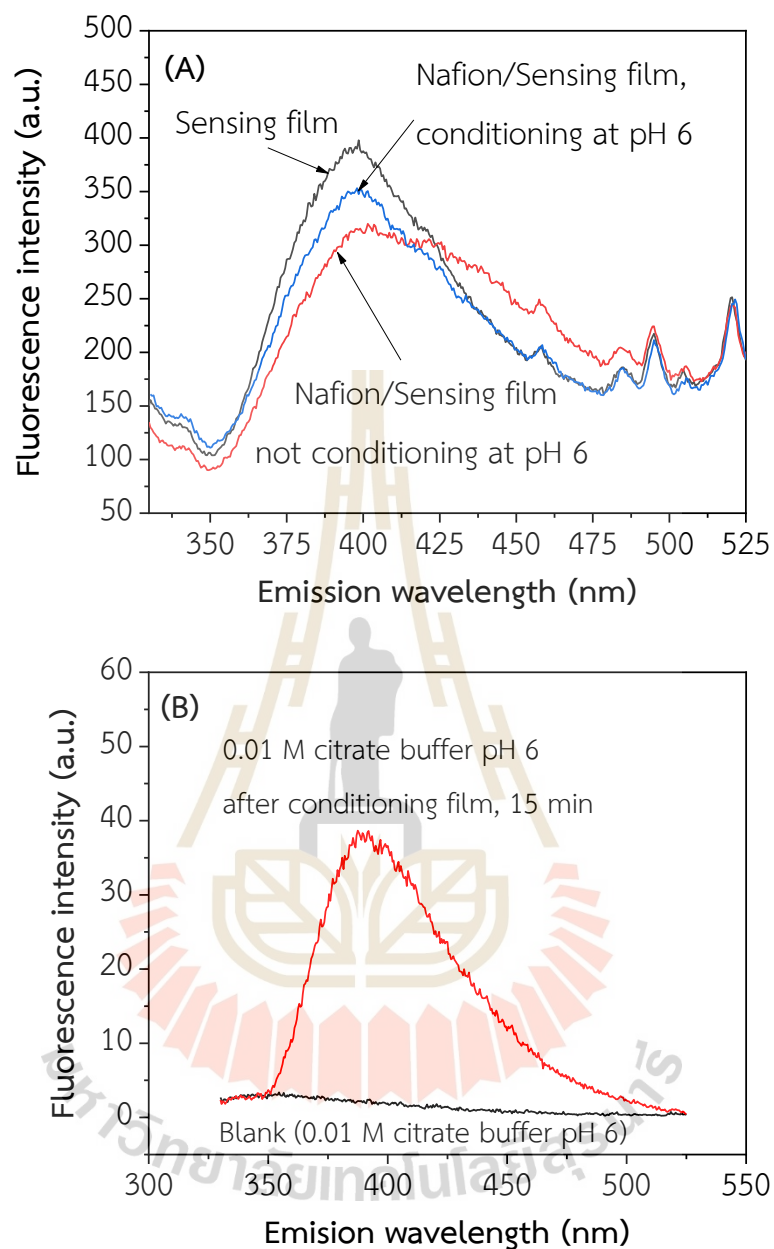
Figure 4.22 Fluorescence emission spectra of (A) the sensing film before and after coating with Nafion and the Nafion-coated film after soaking in 0.01 M citrate buffer pH 6 and (B) 0.01 M citrate buffer after removing the Nafion-coated film.

The excess BPS from the Nafion-coated BPS-NH$_2$-MSF can be removed by immersing the film in 40.0 mL of 0.01 M citrate buffer pH 6 for 15 min. Figures 4.23(A) and 4.23(B) show the fluorescence intensity at 395 nm of the sensing film and 0.01 M citrate buffer pH 6 before and after removing the excess BPS, respectively. The results show that the fluorescence intensity of the film before and after removing the excess BPS is about the same. The results suggested that Nafion coating contributed significantly to reducing BPS leaching. In the solution, a slight fluorescence intensity at 395 nm was observed after the first removal of the excess BPS, and it further decreased after the second removal. This observation is similar to the signal in the blank solution. This result confirms that excess BPS can be removed from the film by soaking the film in a citrate buffer.
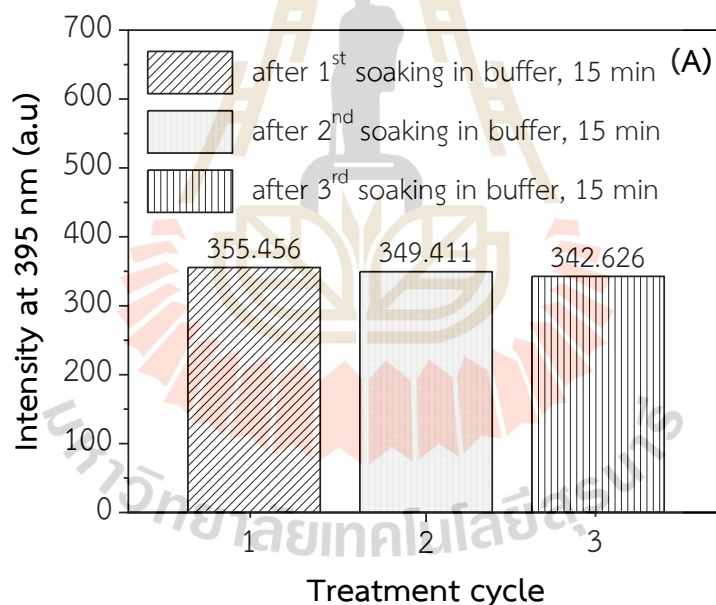
Figure 4.23 Fluorescence intensity at 395 nm of (A) Nafion-coated BPS-NH$_2$-MSF before and after soaking in 0.01 M citrate buffer pH 6 and (B) 0.01 M citrate buffer pH 6 before and after film removal.
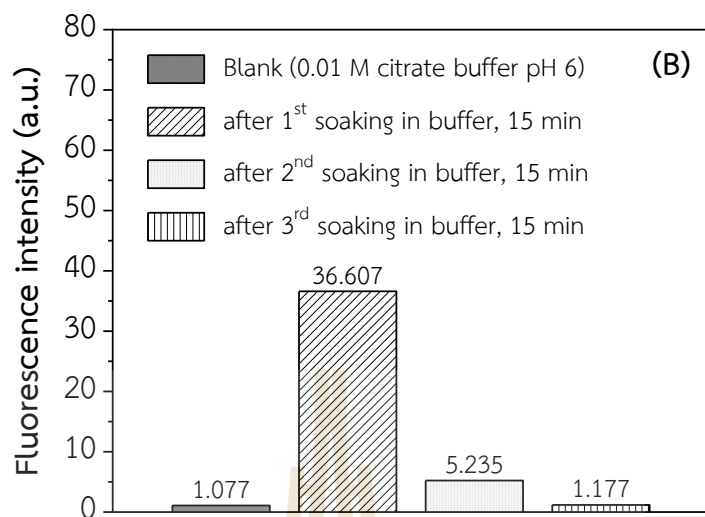
Figure 4.23 Fluorescence intensity at 395 nm of (A) Nafion-coated BPS-NH$_2$-MSF before and after soaking in 0.01 M citrate buffer pH 6 and (B) 0.01 M citrate buffer pH 6 before and after film removal (continued).

4.9.2 Reproducibility of Nafion-coated BPS-NH$_2$-MSF preparation

The reproducibility of the Nafion/BPS-NH$_2$-MSF preparation was investigated by measuring the fluorescence signal at 395 nm after removing excess BPS and conditioning in 0.01 M citrate buffer pH 6. Figures 4.24 show the fluorescence intensity of eight sensing films from three synthesis gel batches. The results demonstrate that the preparation of the sensing film was reproducible, with a relative standard deviation of 5.85% for all batches combined and 4.42%, 4.49%, and 7.19% for the first, second, and third batches, respectively.
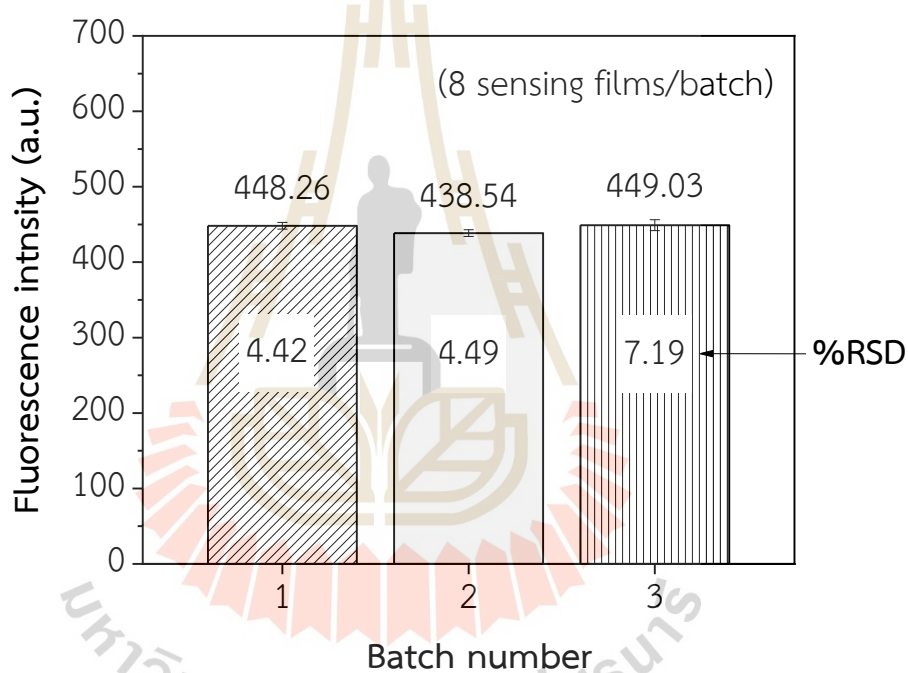
Figure 4.24 Fluorescence intensity at 395 nm of Nafion/BPS-NH$_2$-MSFs prepared from the three batches of the sol-gel mixture.

4.10 Performance characteristics of Nafion-coated sensing film

4.10.1 Response of Nafion-coated BPS-NH$_2$-MSF to Ni^{2+}

The response of Nafion-coated sensing film to Ni^{2+} was studied in the Ni^{2+} concentration range of 5 to 40 ppm. Figure 4.25 shows the time profile signals of the sensing films in Ni^{2+} solutions. The response was reported as the relative signal response, I$_0$ - I/I$_0$, versus response time, where I$_0$ is the fluorescence signal at 395 nm of the film after conditioning with 0.01 M citrate buffer for 15 min and I is the fluorescence signal of the film at 395 nm after exposure to Ni^{2+} at different time. The results indicated that the fluorescence quenching increased Ni^{2+} concentration. The films responded to Ni^{2+} relatively fast, reaching a steady state after about 30 s.
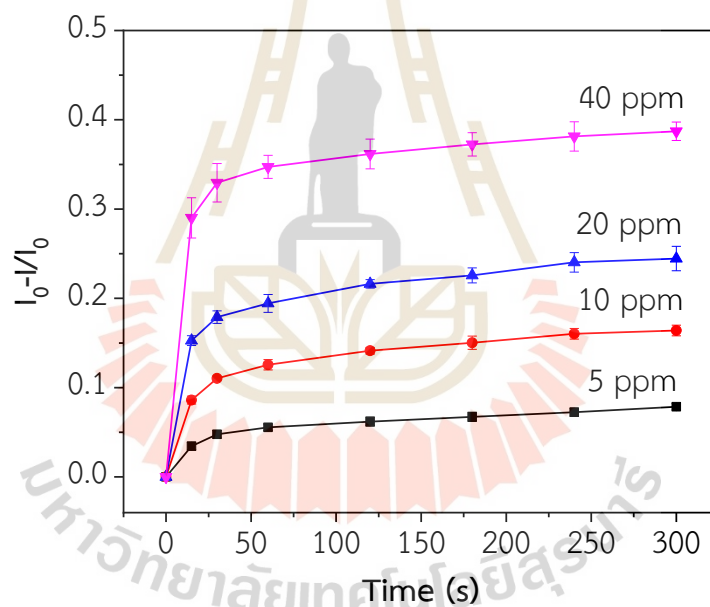
Figure 4.25 Time profiles of response signal at 395 nm of the Nafion-coated sensing films with different concentrations of Ni^{2+}. The solution pH was fixed at 6 using 0.01 M citrate buffer.

4.10.2 Calibration curve for Ni^{2+}

The fluorescence quenching of BPS by Ni^{2+} can be express by using the Stern-Volmer Equation (4.1) as follows:

$$I_0 / I = 1 + K_{sv} [Ni^{2+}] \qquad (4.1)$$

where I_0 is the fluorescence signal of the film after conditioning with 0.01 M citrate buffer for 15 min, I is the fluorescence signal of the film after exposure to Ni^{2+} for 30 s , K_{sv} is the Stern-Volmer quenching constant, and $[Ni^{2+}]$ is the concentration of Ni^{2+}.

The Stern-Volmer plot is shown in Figure 4.26. A linear calibration was obtained in the 5-40 ppm Ni^{2+}. The regression equation is y = 0.0122X + 0.0014, with a correlation coefficient (R^2) 0.9907. The limit of detection (LOD) was found to be 2.45 ppm, as defined in Equation (4.2):

$$LOD = 3s_{bk} / m \qquad (4.2)$$

where s_{bk} is the standard deviation of the blank signal and m is the slope of the Stern-Volmer plot.
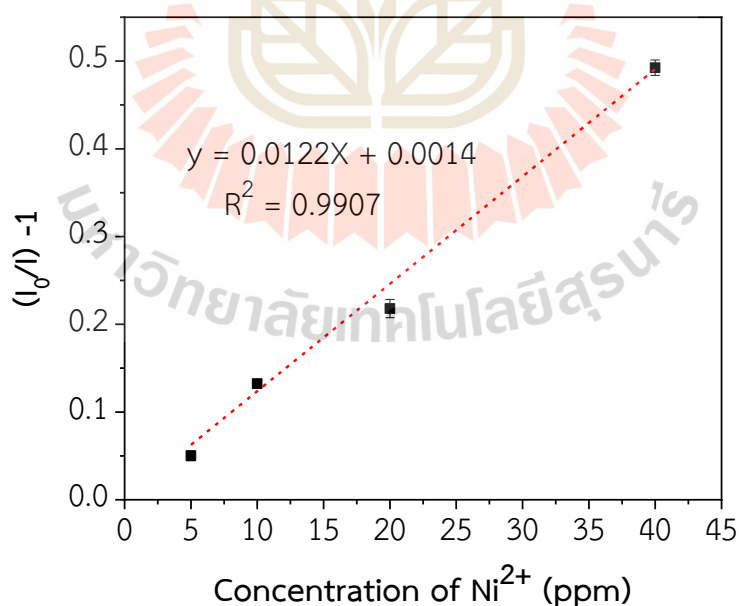
Figure 4.26 Calibration curve for Ni^{2+}.

4.10.3 Reproducibility and regeneration

The reproducibility of the sensing films in response to Ni^{2+} was evaluated by measuring the fluorescence signal of three sensing films in 5 ppm Ni^{2+} solution and another three sensing films in 40 ppm Ni^{2+} solution for 30 seconds. Figure 4.27(A) shows that the films responded reproducibly at both Ni^{2+} concentrations, with the corresponding RSD values of 0.54% for 5 ppm and 3.22% for 40 ppm.

The regeneration of a sensor refers to restoring the fluorescence signal to its original or near-original signal. After the sensor was contacted with Ni^{2+} solution, it was immersed in 0.1 M EDTA to remove Ni^{2+} and then conditioned in 0.01 M citrate buffer pH 6. Figure 4.26(B) shows the signals of the sensing films after regeneration 3 times. The results indicated that the EDTA solution could efficiently remove Ni^{2+} from the sensing film. The fluorescence signal of the regenerated film was found to return to near the initial fluorescence intensity with the RSD of 1.40%.
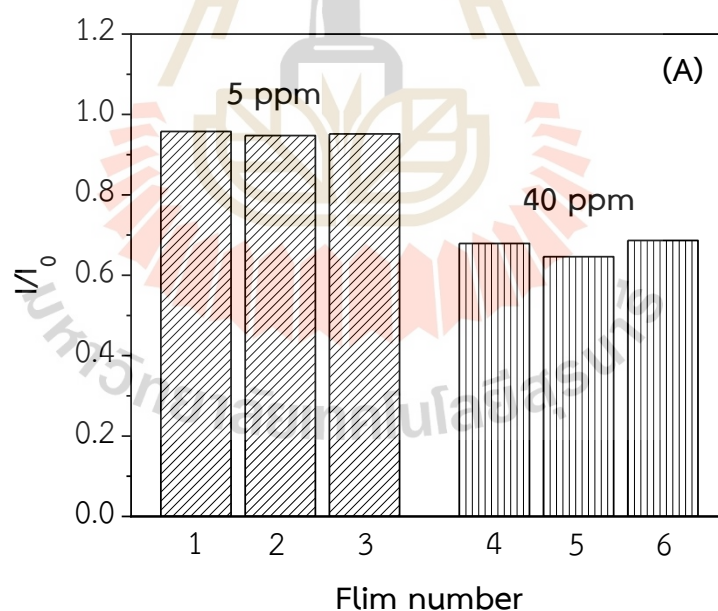
Figure 4.27 (A) Reproducibility and (B) regeneration of the Nafion-coated sensing film.
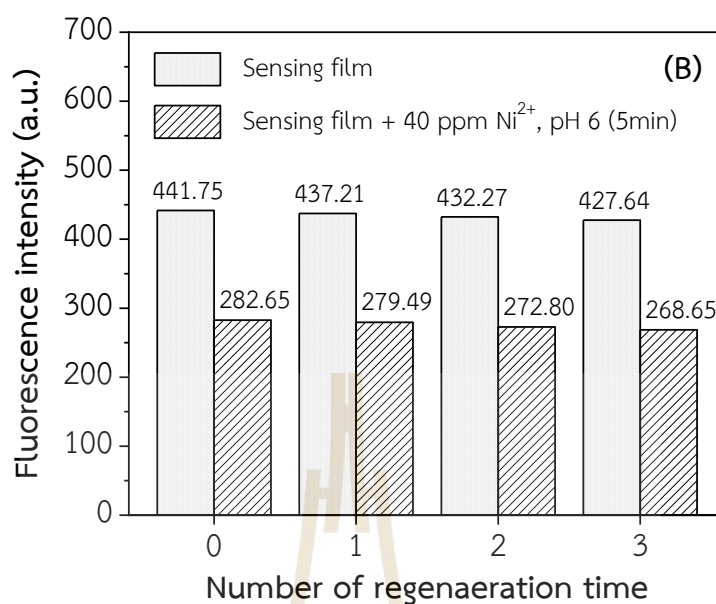
Figure 4.27 (A) Reproducibility and (B) regeneration of the Nafion-coated sensing film (continued).

4.10.4 Interference study

The effect of foreign species, Co^{2+}, Cu^{2+}, Zn^{2+}, and Mg^{2+}, on the response of the sensing films to Ni^{2+} was studied. Fluorescence signal measurements were made in Ni^{2+} solutions with and without the tested species. The molar ratio of Ni^{2+} to the tested species was 1:5. Ni^{2+} concentration was fixed at 0.17 mM. The pH of the solutions were fixed at 6 with citrate buffer. The changes in the fluorescence signal of the sensing film in the presence of the tested species were expressed %error defined as Equation (4.3) and the results are displayed in Table 4.1. From the study, Zn^{2+} interfered the measurement significantly. However, the consideration of interference species also depends on the concentration and the existence of the interference species in the samples.

$$\%error = [(I_{r,\ Ni^{2+}/tested\ ion} - I_{r,\ Ni^{2+}})\ /I_{r,\ Ni^{2+}}] \times 100 \tag{4.3}$$

where I_r is the relative intensity defined as I/I_0, $I_{r, Ni^{2+}/tested\ ion}$ is the relative intensity of the film in a Ni^{2+} solution with the tested ion and $I_{r, Ni^{2+}}$ is the relative intensity of the film in a Ni^{2+} solution without the tested ion.

Table 4.1 Interference study at a 1:5 molar ratio of Ni^{2+} to the tested species.

Tested species	%Error
Co^{2+}	1.91
Cu^{2+}	2.97
Zn^{2+}	11.66
Mg^{2+}	1.78

4.10.5 Real sample analysis

The prepared Nafion-coated sensing film was applied to quantify Ni^{2+} in tap water samples to demonstrate the applicability of the developed sensor. The results are shown in Table 4.2. The developed method could not detect Ni^{2+} in the samples. Ni^{2+} is generally not found in tap water samples, so the sample was spiked with a known amount of Ni^{2+}. The recovery and RSD value suggested that the proposed method was reliable for Ni^{2+} determination. The proposed method and the other optical chemical sensors for Ni^{2+} are compared in Table 4.3. Although the developed method gave a high detection limit for Ni^{2+}, the sensor has the advantages of rapid response to Ni^{2+} and the potential for reusable.

Table 4.2 Determination of Ni^{2+} in the tap water sample.

Sample	Ni^{2+} added, ppm	Ni^{2+} found, ppm ±SD (n=3)	%Recovery	%RSD
Tap water	0	not detect	-	-
	10.0	10.2±0.4	102	3.83

Table 4.3 Comparison of the developed sensor and other sensors in the literature.

Sensing reagent	Supporting matrix	Mode of measurement	Limit of detection	Response time
2-amino-1-cyclopentene-1-dithiocarboxylic acid[a]	Acetyl cellulose membrane	Absorbance	5.2×10^{-7} M	10 min
2,5-thiophenylbis(5-tert-butyl-1,3-benzexazole)[b]	PVC membrane	Fluorescence	8.0×10^{-9} M	< 40 s
2-(5-bromo-2-pyridylazo)-5-(diethylamino)phenol[c]	Nafion membrane	Absorbance	2.0×10^{-7} M	3 min
3,7-diamine-5-phenothiazoniom thionineacetate[d]	Agarose membrane	Absorbance	9.3×10^{-11} M	3 min
2-6-(3-methyl-3-mesitylcyclobutyl)-thiazolo [3,2-b][1,2,4]triazol-2-yl-phenol[e]	PVC membrane	Fluorescence	8.5×10^{-10} M	2 min
3-hydroxy-3-phenyl triaz-1-en-1-benzoic acid[f]	Agarose membrane	Absorbance	2.74×10^{-6} M	10 min
BPS (This work)	Mesoporous silica film/FTO	Fluorescence (quenching)	4.14×10^{-5} M	30 s

[a]Ensafi and Bakhshi (2003), [b]Shamsipur et al. (2004), [c]Amini et al. (2004), [d]Hashemi et al. (2011), [e]Aksuner et al. (2012), and [f]Rasolzadeh et al. (2019)

CHAPTER V

CONCLUSIONS

The optical chemical sensor based on BPS immobilized on modified MSF was successfully developed for the determination of Ni^{2+}. MSFs with various thicknesses were synthesized on FTO using the EASA method, which involved applying a potential step of -1.3 V for 30 seconds. The obtained MSFs had a well-ordered mesostructure with hexagonal packing and vertical orientation of mesopore channels. MSFs with amino modification were used as a supporting material for immobilizing BPS. The films were modified with 3-aminopropyl triethoxysilane by co-condensation in the synthesis mixture and post-grafting route. More BPS was immobilized on the amino-modified films using the post-grafting method and the chosen time for dye immobilization was 18 h. The BPS-immobilized sensing film was characterized by fluorescence spectroscopy and showed an emission wavelength of 395 nm with an excitation wavelength of 285 nm. The sensing film fabricated from four layered MSF exhibited fluorescence quenching upon exposure to Ni^{2+} solutions buffered at pH 6. However, BPS leached from the sensing film. The film also contained some aggregates of silica particles.

A Nafion coating was used to prevent reagent leaching from the sensing film. In addition, synthesis with a lower deposition of 15 seconds was used to reduce silica aggregates on the films. Two layered MSFs with amino modification were used for BPS immobilization. The BPS-immobilized films were coated with Nafion and tested for their response to Ni^{2+}. These sensing films responded rapidly to Ni^{2+} solutions pH 6 with no evidence of dye leaching. The response signal approached equilibrium values in about 30 seconds. The developed method provided a linear response to Ni^{2+} in a concentration range of 5-40 ppm, with a detection limit of 2.45 ppm. The Nafion-coated sensing film, after exposure to Ni^{2+} could be regenerated in an EDTA solution.
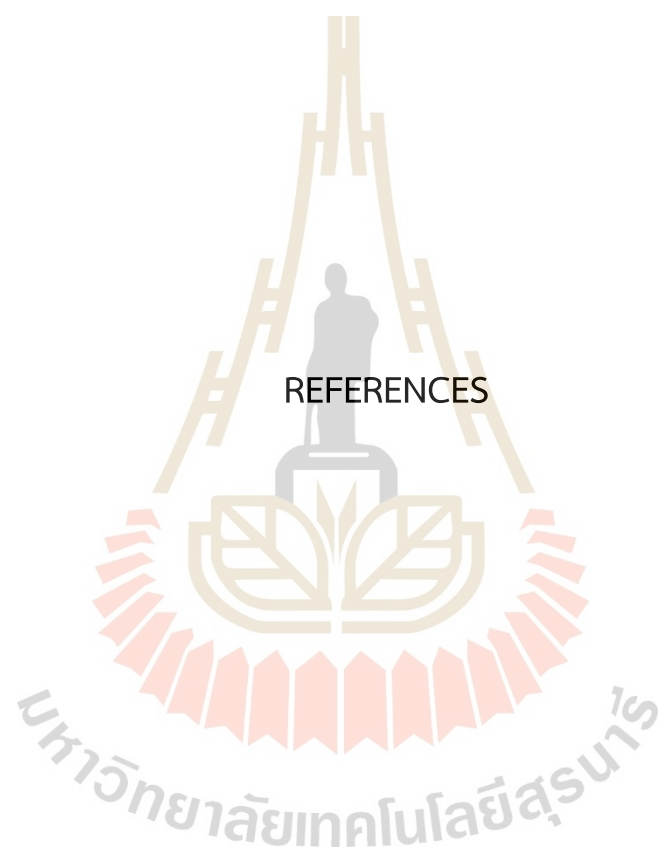
REFERENCES

REFERENCES

Ahuja, D., and Parande, D. (2012). Optical sensors and their applications. *Journal of Scientific Research and Reviews, 1*(5), 060-068.

Aksuner, N., Henden, E., Yilmaz, I., and Cukurovali, A. (2012). A novel optical chemical sensor for the determination of nickel(II) based on fluorescence quenching of newly synthesized thiazolo-triazol derivative and application to real samples. *Sensors and Actuators B: Chemical, 166-167*, 269-274.

Amini, M. K., Momeni-Isfahani, T., Khorasani, J. H., and Pourhossein, M. (2004). Development of an optical chemical sensor based on 2-(5-bromo-2-pyridylazo)-5-(diethylamino)phenol in Nafion for determination of nickel ion. *Talanta, 63*(3), 713-720.

Aragay, G., Pons, J., and Merkoci, A. (2011). Recent trends in macro-, micro-, and nanomaterial-based tools and strategies for heavy-metal detection. *Chemical Reviews, 111*(5), 3433-3458.

Calvo, A., Joselevich, M., Soler-Illia, G. J. A. A., and Williams, F. J. (2009). Chemical reactivity of amino-functionalized mesoporous silica thin films obtained by co-condensation and post-grafting routes. *Microporous and Mesoporous Materials, 121*(1-3), 67-72.

de O. N. Ribeiro, J., Nunes, E. H. M., Vasconcelos, D. C. L., Vasconcelos, W. L., Nascimento, J. F., Grava, W. M., and Derks, P. W. J. (2019). Role of the type of grafting solvent and its removal process on APTES functionalization onto SBA-15 silica for CO_2 adsorption. *Journal of Porous Materials, 26*(6), 1581-1591.

Ding, L., Li, W., Sun, Q., He, Y., and Su, B. (2014). Gold nanoparticles confined in vertically aligned silica nanochannels and their electrocatalytic activity toward ascorbic acid. *Chemistry, 20*(40), 12777-12780.

Ding, L., and Su, B. (2015). An electrochemistry assisted approach for fast, low-cost and gram-scale synthesis of mesoporous silica nanoparticles. *RSC Advances, 5*(81), 65922-65926.

Ensafi, A. A., and Bakhshi, M. (2003). New stable optical film sensor based on immobilization of 2-amino-1-cyclopentene-1-dithiocarboxylic acid on acetyl cellulose membrane for Ni(II) determination. *Sensors and Actuators B: Chemical, 96*(1-2), 435-440.

Etienne, M., Goux, A., Sibottier, E., and Walcarius, A. (2009). Oriented mesoporous organosilica films on electrode: a new class of nanomaterials for sensing. *Journal of Nanoscience and Nanotechnology, 9*(4), 2398-2406.

Feng, D., Wei, J., Wang, M., Yue, Q., Deng, Y., Asiri, A. M., and Zhao, D. (2013). Advances in Mesoporous Thin Films via Self-Assembly Process. *Advanced Porous Materials, 1*, 164-186.

Giordano, G., Vilà, N., Aubert, E., Ghanbaja, J., and Walcarius, A. (2017). Multi-layered, vertically-aligned and functionalized mesoporous silica films generated by sequential electrochemically assisted self-assembly. *Electrochimica Acta, 237*, 227–236.

Goux, A., Etienne, M., Aubert, E., Lecomte, C., Ghanbaja, J., and Walcarius, A. (2009). Oriented Mesoporous Silica Films Obtained by Electro-Assisted Self-Assembly (EASA). *Chemistry of Materials, 21*, 731-741.

Hashemi, P., Hosseini, M., Zargoosh, K., and Alizadeh, K. (2011). High sensitive optode for selective determination of Ni^{2+} based on the covalently immobilized thionine in agarose membrane. *Sensors and Actuators B: Chemical, 153*(1), 24-28.

Hirayama, T., and Nagasawa, H. (2017). Chemical tools for detecting Fe ions. *Journal of Clinical Biochemistry and Nutrition, 60*(1), 39-48.

Hoffmann, F., Cornelius, M., Morell, J., and Froba, M. (2006). Silica-based mesoporous organic-inorganic hybrid materials. *Angew Chem Int Ed Engl, 45*(20), 3216-3251.

Korent Urek, Š., Frančič, N., Turel, M., and Lobnik, A. (2013). Sensing Heavy Metals Using Mesoporous-Based Optical Chemical Sensors. *Journal of Nanomaterials, 2013*, 1-13.

Rasolzadeh, F., Hashemi, P., and Rezaei, B. (2019). Aryl triazene derivative immobilized on agarose membrane for selective optical sensing and quantitation of Ni^{2+} in water. *Journal of the Iranian Chemical Society, 16*(6), 1283-1289.

Sakamoto, M., Hizava, K., Hosaka, M., and Sugawara, M. (2016). Visual Assay of Total Iron in Human Serum with Bathophenanthrolin Disulfonate-accommodated MCM-41. *Analytical Sciences, 32*, 241-244.

Shamsipur, M., Poursaberi, T., Karami, A. R., Hosseini, M., Momeni, A., Alizadeh, N., Yousefi, M., and Ganjali, M. R. (2004). Development of a new fluorimetric bulk optode membrane based on 2,5-thiophenylbis(5-tert-butyl-1,3-benzexazole) for nickel(II) ions. *Analytica Chimica Acta, 501*(1), 55-60.

Soler-Illia, G. J. A. A., Angelomé, P. C., Fuertes, M. C., Calvo, A., Wolosiuk, A., Zelcer, A., Bellino, M. G., and Martínez, E. D. (2010). Mesoporous hybrid and nanocomposite thin films. A sol–gel toolbox to create nanoconfined systems with localized chemical properties. *Journal of Sol-Gel Science and Technology, 57*(3), 299-312.

Story, J. N. (1973). *I. Application of 1,10-phenanthroline to the spectrophotofluorometric analysis of zinc and cadmium; II. Partially sulfonated, macroreticular ion exchange resins in the separation of metal ions.* (Ph.D. Retrospective Theses and Dissertations). Iowa State University, Digital Repository @ Iowa State University.

Talavera-Pech, W. A., Esparza-Ruiz, A., Quintana-Owen, P., Vilchis-Nestor, A. R., Carrera-Figueiras, C., and Ávila-Ortega, A. (2016). Effects of different amounts of APTES on physicochemical and structural properties of amino-functionalized MCM-41-MSNs. *Journal of Sol-Gel Science and Technology, 80*(3), 697-708.

Teng, Z., Zheng, G., Dou, Y., Li, W., Mou, C. Y., Zhang, X., Asiri, A. M., and Zhao, D. (2012). Highly ordered mesoporous silica films with perpendicular mesochannels by a simple Stober-solution growth approach. *Angew Chem Int Ed Engl, 51*(9), 2173-2177.

Urbanova, V., and Walcarius, A. (2014). Vertically-aligned Mesoporous Silica Films. *Zeitschrift für anorganische und allgemeine Chemie, 640*(3-4), 537-546.

van de Weert, M., and Stella, L. (2011). Fluorescence quenching and ligand binding: A critical discussion of a popular methodology. *Journal of Molecular Structure, 998*(1-3), 144-150.

Walcarius, A. (2015). Mesoporous Materials-Based Electrochemical Sensors. *Electroanalysis, 27*(6), 1303-1340.

Walcarius, A., Sibottier, E., Etienne, M., and Ghanbaja, J. (2007). Electrochemically assisted self-assembly of mesoporous silica thin films. *Nature Materials, 6*(8), 602-608.
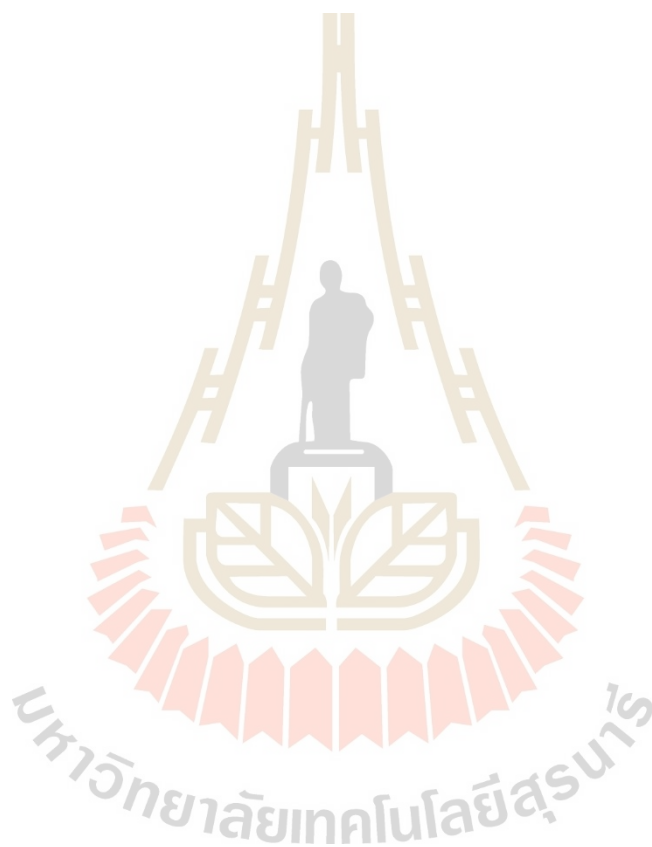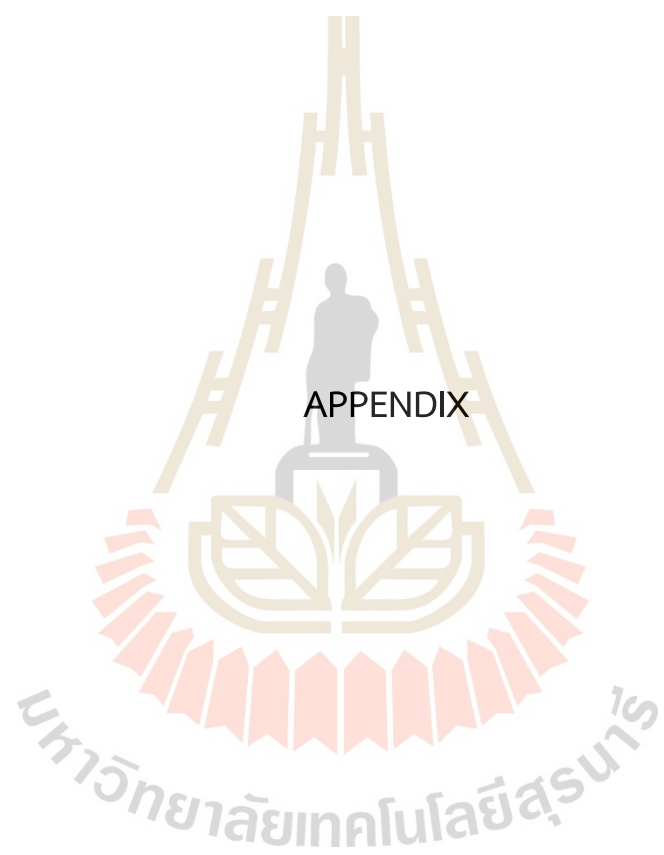
APPENDIX

APPENDIX

REDOX PROBES FOR CHARACTERIZATION OF

MESOPOROUS SILICA FILMS

Ruthenium hexaamine ion, $Ru(NH_3)_6^{3+}$, and iron hexacyanoferrate, $Fe(CN)_6^{3-}$, were used to characterize the permeability of mesoporous silica films by cyclic voltammetry. The two species are known for the reversible redox couple behavior and the ability to move through the hexagonal mesoporous channels to interact with the underlying electrode surface. Half-reactions involving the probe species are shown in Equations (A1) and (A2). The redox reactions depend on the presence/absence of the surfactant template and the charge on the surface of the mesoporous channels.

$$Ru(NH_3)_6^{3+} + e^- \rightleftharpoons Ru(NH_3)_6^{2+} \qquad\qquad (A1)$$

$$Fe(CN)_6^{3-} + e^- \rightleftharpoons Fe(CN)_6^{4-} \qquad\qquad (A2)$$
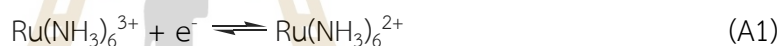
CURRICULUM VITAE

NICHAKORN PORNNONGSAN

Education

2013 - 2017   B.Sc. in Environment Health, Suranaree University of
                     Technology, Thailand

2018 - present   M.Sc. candidate in Chemistry, Suranaree University of
                     Technology, Thailand

Scholarship

2018 - 2020   Kittibanndit scholarships, Suranaree University of Technology

Publication

Pornnongsan, N., Sombatsri, S., Rongchapo, W., Deekamwong, K., and Prayoonpokarach,
S., (2021). *Preparation of Amino-Functionalized Mesoporous Silica Film
Using Electrochemically Assisted Self-Assembly for Immobilization of
Bathophenantroline Disulfonate.* In Proceedings of SUT International
Virtual Conference on Science and Technology, Suranaree University of
Technology, Thailand.